J Neurophysiol 104: 2713–2729, 2010.
First published September 8, 2010; doi:10.1152/jn.00334.2010.

Late-Expiratory Activity: Emergence and Interactions With the Respiratory CPG

Yaroslav I. Molkov,[1] Ana P. L. Abdala,[2] Bartholomew J. Bacak,[1] Jeffrey C. Smith,[3] Julian F. R. Paton,[2] and Ilya A. Rybak[1]

[1]*Department of Neurobiology and Anatomy, Drexel University College of Medicine, Philadelphia, Pennsylvania;* [2]*Department of Physiology and Pharmacology, Bristol Heart Institute, School of Medical Sciences, University of Bristol, Bristol, United Kingdom; and* [3]*Cellular and Systems Neurobiology Section, National Institute of Neurological Disorders and Stroke, National Institutes of Health, Bethesda, Maryland*

Submitted 12 April 2010; accepted in final form 8 September 2010

Molkov YI, Abdala APL, Bacak BJ, Smith JC, Paton JFR, Rybak IA. Late-expiratory activity: emergence and interactions with the respiratory CPG. *J Neurophysiol* 104: 2713–2729, 2010. First published September 8, 2010; doi:10.1152/jn.00334.2010. The respiratory rhythm and motor pattern are hypothesized to be generated by a brain stem respiratory network with a rhythmogenic core consisting of neural populations interacting within and between the pre-Bötzinger (pre-BötC) and Bötzinger (BötC) complexes and controlled by drives from other brain stem compartments. Our previous large-scale computational model reproduced the behavior of this network under many different conditions but did not consider neural oscillations that were proposed to emerge within the retrotrapezoid nucleus/parafacial respiratory group (RTN/pFRG) and drive preinspiratory (or late-expiratory, late-E) discharges in the abdominal motor output. Here we extend the analysis of our previously published data and consider new data on the generation of abdominal late-E activity as the basis for extending our computational model. The extended model incorporates an additional late-E population in RTN/pFRG, representing a source of late-E oscillatory activity. In the proposed model, under normal metabolic conditions, this RTN/pFRG oscillator is inhibited by BötC/pre-BötC circuits, and the late-E oscillations can be released by either hypercapnia-evoked activation of RTN/pFRG or by hypoxia-dependent suppression of RTN/pFRG inhibition by BötC/pre-BötC. The proposed interactions between BötC/pre-BötC and RTN/pFRG allow the model to reproduce several experimentally observed behaviors, including quantal acceleration of abdominal late-E oscillations with progressive hypercapnia and quantal slowing of phrenic activity with progressive suppression of pre-BötC excitability, as well as to predict a release of late-E oscillations by disinhibition of RTN/pFRG under normal conditions. The extended model proposes mechanistic explanations for the emergence of RTN/pFRG oscillations and their interaction with the brain stem respiratory network.

INTRODUCTION

Rhythmic movements such as breathing and locomotion are produced by central pattern generators (CPGs) that can generate rhythmic activity without periodical patterned inputs or feedback (Grillner et al. 2005; Marder and Calabrese 1996). The rhythmic activities generated emerge from a combination of cellular properties of the neurons comprising the CPG and synaptic interactions among these neurons. In addition, the CPGs are incorporated into larger neural systems and operate under control of various central and peripheral sensory inputs and drives that modify the CPG-generated motor pattern, adjusting it to the internal and/or external environment, current motor task, and organismal needs. External sustained drives to particular circuit elements may control the CPG operation by changing the balance of neuronal interactions thereby changing the frequency and/or amplitude of motor outputs. Such inputs can even reconfigure the CPG dramatically changing the operational rhythmogenic and pattern formation mechanisms (e.g., Rubin et al. 2009; Smith et al. 2007). Another qualitatively different control of CPG operation can be performed by external state-dependent oscillations the characteristics of which (e.g., frequency and/or phase) carry specific information on the system's state. These external oscillations may affect/control the CPG via various synchronization, coupling and/or entrainment mechanisms. Such "synchronization-based" interactions, as an alternative to "connectivity-based" interactions described above, have been found to play an important role in sensory processing [in the visual (Singer 1993), somatosensory (Bauer et al. 2006), olfactory (Kay et al. 2009), and other sensory systems], central brain mechanisms (Bazhenov et al. 1999; Tort et al. 2008), and neural control of movements (Baker et al. 1999; Grillner et al. 2005). Revealing the mechanisms underlying such oscillatory interactions in the context of the synchronization-based control of CPGs would significantly extend current understanding of the general principles of CPG-based control of rhythmic movements and processes in the brain.

The respiratory cycle in mammals consists of two major phases: inspiration (I) and expiration (E) which in turn is comprised of two phases, postinspiration (post-I or phase E1) and phase E2 (Cohen 1979; Richter 1996). These respiratory phases can be recognized in the integrated activities of the phrenic (PN, defining I phase) and cranial nerves (e.g., laryngeal expressing activity during both inspiration and postinspiration). The respiratory rhythm and coordinated motor pattern are generated by a respiratory CPG located in the lower brain stem (Bianchi et al. 1995; Cohen 1979; Richter 1996; Richter and Spyer 2001). The pre-Bötzinger complex (pre-BötC), located within the medullary ventrolateral respiratory column, is considered a major source of rhythmic inspiratory activity (Feldman and Del Negro 2006; Koshiya and Smith 1999; Rekling and Feldman 1998; Smith et al. 1991). The pre-BötC, interacting with the adjacent Bötzinger complex (BötC) containing mostly expiratory neurons (Cohen 1979; Ezure 1990; Ezure et al. 2003; Jiang and Lipski 1990; Tian et al. 1999) has been considered to represent a core of the respiratory CPG (Bianchi et al. 1995; Cohen 1979; Richter 1996; Richter and

Address for reprint requests and other correspondence: I. A. Rybak, Dept. of Neurobiology and Anatomy, Drexel University College of Medicine, 2900 Queen Ln., Philadelphia, PA 19129 (E-mail: rybak@drexel.edu).

Spyer 2001; Rubin et al. 2009; Rybak et al. 2004, 2007, 2008; Smith et al. 2000, 2007, 2009; Tian et al. 1999). The respiratory oscillations generated by the core circuitry are supposed to be defined by the intrinsic biophysical properties of respiratory neurons involved, the synaptic interactions between respiratory neural populations within and between the pre-BötC and BötC, and input drives from other brain stem compartments including the pons, retrotrapezoid nucleus (RTN), raphé, and nucleus tractus solitarii (NTS). In addition, information on the metabolic state of the system such as levels of CO_2, O_2, pH, provided by the RTN, raphé, peripheral chemoreceptors (via NTS), can reorganize the respiratory network and operating rhythmogenic mechanisms depending on metabolic conditions.

A distinct site of neural oscillations, the parafacial respiratory group (pFRG), putatively involved in respiratory function was initially identified in vitro in the isolated neonatal rat brain stem-spinal cord preparation (Onimaru and Homma 1987, 2003; Onimaru et al. 1988). The pFRG seems to reside within, or to overlap with, RTN. It has been proposed that RTN/pFRG oscillations drive abdominal motor activity, expressing preinspiratory (or late-expiratory, late-E) or biphasic-E (with pre- and postinspiratory) discharges in the abdominal motor output when the system operates in the active expiration state to force exhalation (Abdala et al. 2009a; Feldman and Del Negro 2006; Janczewski and Feldman 2006; Janczewski et al. 2002). Several competing concepts concerning the physiological role of RTN/pFRG oscillations have been suggested and debated (Feldman and Janczewski 2006). These include the suggestion that the pFRG represents the primary inspiratory oscillator (Onimaru and Homma 2003; Onimaru et al. 2006) and the dual oscillator concept that considers the RTN/pFRG to be an independent expiratory rhythm generator that is coupled with a distinct inspiratory rhythm generator in the pre-BötC (Janczewski and Feldman 2006). However, the exact physiological role of pFRG oscillations, the specific conditions for their emergence, and the nature and mechanisms of the interactions between the BötC/pre-BötC and RTN/pFRG oscillators are not yet known.

In this study, we analyze our previous results (Abdala et al. 2009a) and some new experimental data providing additional evidence for the location of the source of abdominal late-E oscillations in RTN/pFRG and the dependence of these oscillations on the persistent sodium current. We also consider the metabolic conditions allowing the emergence of late-E oscillations, and the role of these oscillations in coordination of phrenic and hypoglossal motor outputs.

Our previous large-scale computational models of the spatially and functionally organized brain stem respiratory network (Rybak et al. 2007; Smith et al. 2007) were able to reproduce the three-phase respiratory pattern generated under normal conditions as well as its reorganization resulting from multiple experimental perturbations, such as various brain stem transections, application of specific blockers of ionic channels and attenuation of inhibitory synaptic transmission. Based on these modeling studies, we have concluded that the brain stem respiratory network has rhythmogenic capabilities at multiple hierarchical levels, which allows flexible, state-dependent expression of different rhythmogenic mechanisms under different physiological and metabolic conditions and enables a wide repertoire of respiratory behaviors (Abdala et al. 2009a,b; Rybak et al. 2004, 2007, 2008; Smith et al. 2007, 2009).

Our previous modeling studies, however, did not analyze interactions between the respiratory CPG circuits and RTN/pFRG oscillator. In this study, we extend our previous model (Smith et al. 2007) by incorporating additional neuronal circuits involved in the generation of late-E oscillations in the RTN/pFRG and the abdominal motor output. The resultant extended model was used to simulate and analyze several critical regimes of coupling between the BötC/pre-BötC and RTN/pFRG oscillators, including "quantal acceleration" of late-E oscillations with the development of hypercapnia (increasing CO_2 level) and "quantal slowing" of phrenic motor activity with lowered excitability of the pre-BötC.

This study addresses the following issues that are critical for understanding the role of RTN/pFRG oscillations: the metabolic state-dependent conditions allowing for the emergence of RTN/pFRG oscillations, the neuronal connections that may define the specific interactions between BötC/pre-BötC and RTN/pFRG oscillators, and the role of these interactions in the coordination of respiratory motor outputs. Revealing these issues is expected to provide new insights into the state-dependency of RTN/pFRG oscillations, the nature of their coupling with BötC/pre-BötC oscillations, and their impact on respiratory pattern generation under different physiological and pathological conditions.

METHODS

Experimental data

The majority of the data used herein were taken from our recently published study (Abdala et al. 2009a) conducted in the in situ arterially perfused brain stem-spinal cord preparations of juvenile rats. New experimental results presented here included the effects of riluzole, the persistent sodium current blocker, on the abdominal and phrenic motor activities during hypercapnia (increased CO_2 level), and the effect of local blockade of $GABA_A$ergic synaptic inhibition within the RTN/pFRG region on the abdominal late-E activity during normocapnia (baseline level of CO_2). Procedures for applying riluzole (5–10 μM) to the perfusate in the in situ preparations with recording of multi-nerve activities to study the role of this current in respiratory pattern generation in situ have been described in detail in Smith et al. (2007). The procedures used here for local, bilateral injection of bicuculline (a blocker of $GABA_A$ergic synaptic transmission, 10 μM) into the RTN/pFRG, including histological documentation of injection sites, were identical to those described in Abdala et al. (2009a) for focal injection of pharmacological agents perturbing $GABA_A$ergic synaptic transmission in the RTN/pFRG. For all other experimental details, including electrophysiological methods for recording abdominal nerve (AbN) activity simultaneously with activity of cervical vagus (cVN) and hypoglossal (HN) cranial nerves and PN nerve, refer also to Abdala et al. (2009a).

Data processing and analysis

We measured parameters of motor or neuronal unit activity (cycle period/frequency, inspiratory/expiratory phase durations and amplitudes) across ≥50 respiratory cycles. For time-series analysis of different outputs, we used signals simultaneously recorded from nerves and neuronal units digitally acquired (5 kHz sampling rate) by means of Spike2 (Cambridge Electronics Design) software. For detection of nerve bursting activity, these signals were DC removed, rectified, and integrated (50 ms time constant). An appropriate threshold was chosen, and the time points of successive intersections of the integrated activity with the threshold were registered. The time intervals between the onsets or offsets of two successive bursts of nerve activity (referred to as periods) were computed. Processing of digi-

tized data were performed using the software package TESEAN (Hegger et al. 1999) and custom written C++ programs.

Modeling and simulations

The model was developed based on, and as an extension of, the previous model described by Smith et al. (2007). All neurons were modeled in the Hodgkin-Huxley style (single-compartment models) and incorporated known biophysical properties and channel kinetics characterized in respiratory neurons in vitro. Each neuronal type was represented by a population of 50 neurons. Heterogeneity of neurons within each population was set by a random distribution of some parameters and the initial conditions for values of membrane potential, calcium concentrations, and channel conductances. Each neuron of a target population received synaptic inputs from all neurons of a source population and/or a corresponding source of excitatory drive in accordance with network architecture of the model. A full description of the previous model and model parameters used can be found in Smith et al. (2007). All new (additional), and altered (relative to Smith et al. 2007) model parameters are indicated in Table 1.

All simulations were performed with a simulation package NSM 3.0, developed at Drexel University by S. N. Markin, I. A. Rybak, and N. A. Shevtsova. Differential equations were solved using the exponential Euler integration method with a step of 0.1 ms. Other details of the modeling and simulation methods can be found in Rybak et al. (2003b, 2007) and Smith et al. (2007).

RESULTS

In this section, we present results from new analyses of our previously published data (Abdala et al. 2009a) as well as new experimental observations that form the basis for developing an extended computational model of the brain stem respiratory network described in the following section.

Emergence and quantal acceleration of late-E abdominal activity with hypercapnia

Under baseline metabolic conditions (95% O_2-5% CO_2) the abdominal motor output (AbN) recorded in the in situ arterially perfused rat brain stem-spinal cord preparations typically exhibits a low-amplitude postinspiratory activity as described in Abdala et al. (2009a). Switching to hypercapnic (7–10% CO_2) and/or hypoxic (reduced O_2 level) conditions evokes large amplitude late-expiratory (late–E, also called preinspiratory, pre-I) bursts in AbN. A representative example is shown in Fig. 1 where the late-E discharges emerge in AbN at 7% CO_2 (Fig. 1, *A2* and *B*) followed by a progressive increase in their frequency (decrease in the burst period) as the CO_2 concentration is incremented to 10%. Importantly, although the frequency of late-E bursts increases with CO_2, these bursts remain coupled (phase-locked) with the bursts in the PN, cVN, and HN nerves (Fig. 1*A, 2–4,* see also Figs. 2*A, 1* and *3,* and 4, *A, 1* and *2,* and *B*). With the development of hypercapnia, the ratio of late-E burst frequency to the PN burst frequency shows a step-wise or *quantal* increase from 1:5 and 1:4 (seen in Fig. 1*B*) to 1:3, 1:2, and, finally, to 1:1 (Fig. 1, *A, 2–4* and *B*; see also Fig. 4, *A1* and *B*). On returning CO_2 to the control levels, the ratio showed a step-wise reversal (see in Fig. 4*B*). Similar hypercapnia-evoked AbN late-E discharges phase-locked to PN with a step-wise increase of their frequency with increasing CO_2 levels has been demonstrated previously in vivo by Iizuka and Fregosi (2007). We call this process *quantal acceleration* of late-E activity with development of hypercapnia.

Dependence of late-E abdominal bursting on RTN/pFRG

Abdala et al. (2009a) showed that pharmacological suppression of the RTN/pFRG region by local microinjection of isoguvacine, a $GABA_A$ receptor agonist, abolished reversibly the hypercapnia-evoked late-E bursting in the AbN. Figure 2 shows a time series of the oscillation periods of PN and AbN constructed for a representative preparation from the original data set for three sequential activity epochs. During the first epoch, 10% CO_2 was applied to the perfusate, which evoked a quantal distribution of late-E AbN discharge (Fig. 2*A1,* black circles). As shown in the second epoch (Fig. 2*A2*), bilateral microinjections of isoguvacine made in the RTN/pFRG caused transient apnea followed by recovery of PN discharge to the baseline frequency and subsequently blocked late-E AbN bursting during systemic application of 10% CO_2 in the perfusate (no black circles). The third epoch (Fig. 2*A3*) shows recovery of hypercapnia-induced AbN discharge after isoguvacine washout. Based on these experimental data and in agreement with the previous suggestions of others (see Feldman and Del Negro 2006; Janczewski and Feldman 2006; Janczewski et al. 2002), we have hypothesized that the source of hypercapnia-evoked late-E oscillations in AbN is located within RTN/pFRG and that AbN oscillation may be considered as an indicator of the corresponding RTN/pFRG oscillations.

TABLE 1. *Weights of synaptic connections in the network*

Target population (location)	Excitatory Drive {weight of synaptic input} or Source Population {weight of synaptic input from single neuron}
bulbospinal E* (cVRG)	early-I(2) {−2}*; late-E {0.02}*.
ramp-I (rVRG)	drive(pons) {2.0}; early-I(2) {−0.3}*; pre-I/I{0.06}; aug-E{−0.1}*; post-I {−2.0}*.
early-I(2) (rVRG)	drive(pons) {2.5}*; aug-E {−0.25}; post-I {−0.25}*; late-E {0.1}*.
pre-I/I (pre-BötC)	drive(raphé) {0.3}; drive(RTN) {0.22}*; drive(pons) {0.65}*; pre-I/I {0.03}; aug-E {−0.06}*; post-I {−0.16}*; late-E {0.02}*.
late-E* (RTN/pFRG)	early-I(1) {−0.025}*; post-I {−0.0225}*; late-E {0.03}*;
early-I(1) (pre-BötC)	drive (RTN) {1}*; drive(pons) {1.1}; pre-I/I {0.1};* aug-E {−0.265}*; post-I {−0.45}*.
aug-E (BötC)	drive(RTN) {2.1}*; drive(pons) {0.6}*; early-I(1) {−0.115}*; post-I {−0.32}; late-E {0.03}*.
post-I (BötC)	drive(RTN) {0.05}*; drive(pons) {1.65}*; early-I(1) {−0.025}*; aug-E {−0.01}.
post-I (e) (BötC)	drive(pons) {0.05}*; early-I(1) {−0.2}; aug-E {−0.2}*.

Values in brackets represent average relative weights of synaptic inputs from the corresponding source populations (w_{ji}) or drives (w_{dmi}). *, populations not present in the model of Smith et al. (2007) and weights of connections adjusted in the present model relative to that model. cVRG, caudal ventral respiratory group; ramp-I, ramp-inspiratory; early-I(1), early-inspiratory; pre-I/I, preinspiratory/inspiratory; late-E, late-expiratory; aug-E, augmenting-expiratory; post-I, postinspiratory; RTN/pFRG, retrotrapezoid nucleus/parafacial respiratory group; pre-BötC, pre-Bötzinger complex; pre-Bötzinger complex, pre-BötC.

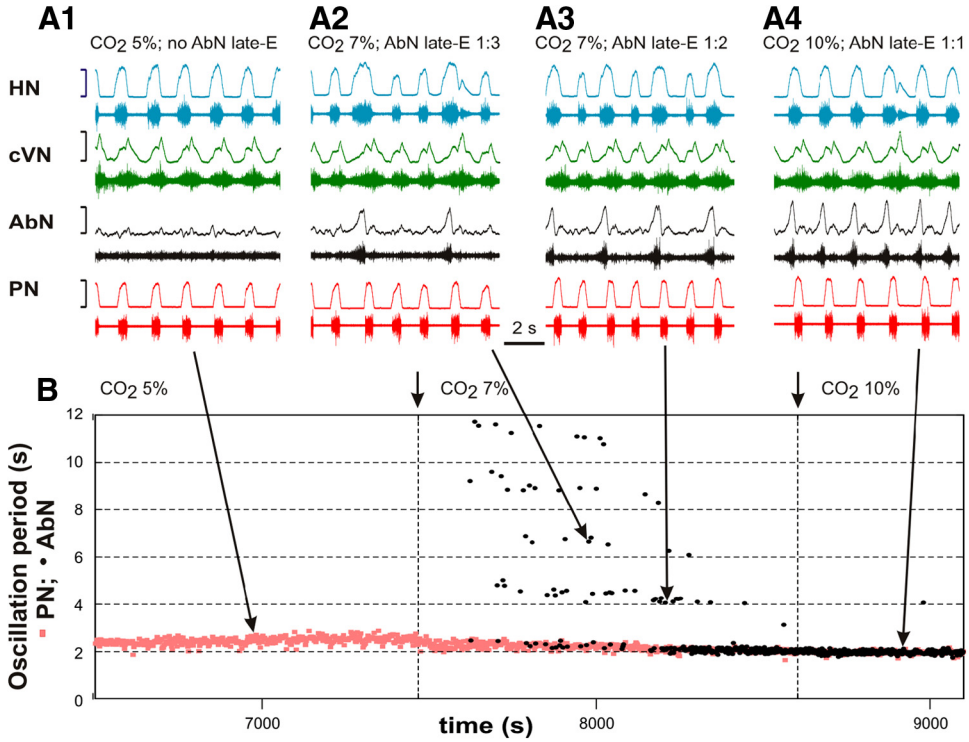

FIG. 1. Quantal acceleration of late-expiratory (late-E) abdominal activity with the development of hypercapnia (increase in the CO_2 concentration in the perfusate). *A, 1–4*: simultaneously recoded activity of (bottom-up) phrenic (PN, red), abdominal (AbN, black), cervical vagus (cVN, green), and hypoglossal (HN, blue) nerves. Activity of each nerve is represented by 2 traces: raw recording (*bottom*) and integrated activity (*top*). *A1*: normocapnia (5% CO_2): late-E activity is absent in the AbN. *A, 2–4*: quantal acceleration of AbN activity: with the development of hypercapnia, the ratio between the AbN and PN frequencies goes through stepwise changes from 1:3 and 1:2 (*A, 2* and *3*, 7% CO_2) to 1:1 (*A4*, 10% CO_2). *B*: time-series representation of the entire experimental epoch with the oscillation periods in the PN (red squares) and AbN (black circles) plotted continuously versus time. The AbN late-E bursts were synchronized with the PN bursts with a ratio increasing quantally from 1:5 to 1:1. The content of CO_2 in the perfusate of this preparation was changed at times indicated by short arrows and vertical dashed lines. Large arrows indicate times corresponding to the episodes shown in *A, 1–4*.

Correlated CO_2-evoked late-E neuron bursting in RTN/pFRG and AbN bursting

Our previous extracellular recordings of single neuron activity in RTN/pFRG indicate that the ventrolateral (vl) part of RTN/pFRG contains a population of CO_2-sensitive neurons that exhibit bursting synchronized with the AbN late-E activity during hypercapnia. Moreover, at 7% CO_2 such neuronal bursts are skipped whenever AbN late-E bursts are skipped, reflecting their relationships (Fig. 3, *A* and *B*). Analysis of the bursting behavior of a set of neurons recorded previously shows that the CO_2-evoked RTN/pFRG neuronal and AbN late-E bursting are highly correlated during hypercapnia. The average probability of simultaneous AbN and RTN/pFRG neuron activity from a group of these neurons ($n = 5$) was 0.92, computed from an average recording epoch of 280 s duration (average number of 141 bursts analyzed per epoch).

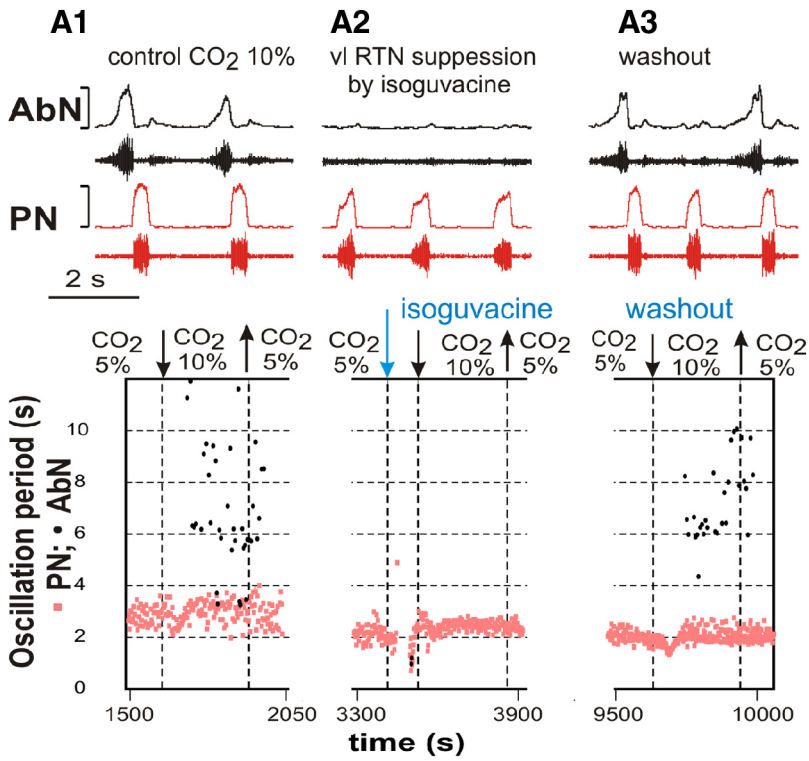

FIG. 2. The effect of retrotrapezoid nucleus/parafacial respiratory group (RTN/pFRG) suppression on hypercapnia-evoked late-E abdominal activity. The ventrolateral (vl) RTN/pFRG region was inactivated by local bilateral microinjection of isoguvacine, a $GABA_A$ receptor agonist. *A, 1–3*: 3 epochs from the same experiment. In each column, the *top diagram* shows the raw recording and integrated activity of PN (*bottom traces,* red) and AbN (*top traces,* black) nerves, and the bottom diagram shows the changes in the oscillation periods in the PN and AbN with time. In *A1,* hypercapnia (10% CO_2) evoked quantally dispersed late-E bursts in AbN (see nerve recordings at the top and black circles in the *bottom diagram*). Note that the time interval was not sufficient to allow development of 1:1 ratio of AbN:PN frequencies. In *A2,* injection of isoguacine fully blocked late-E AbN bursting that would be expected at 10% CO_2 (no black circles). In *A3,* hypercapnia (10% CO_2) again evoked late-E discharges in AbN discharge after isoguvacine washout.

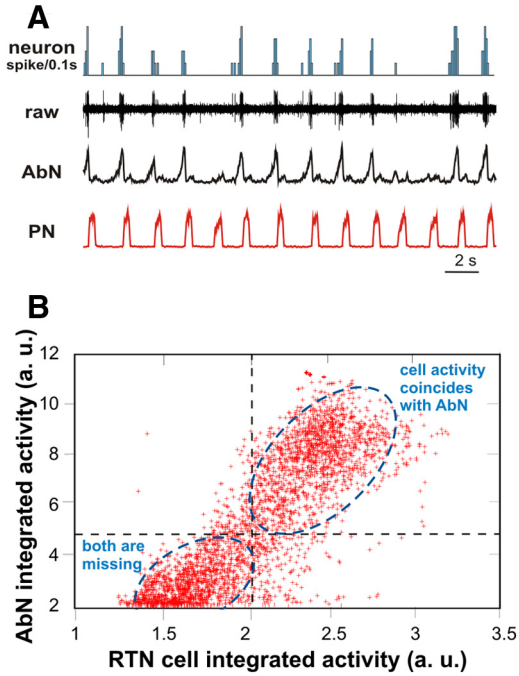

FIG. 3. An example of extracellular recording of a single neuron within the vl part of RTN/pFRG during hypercapnia (7% CO_2), the activity of which correlated with the abdominal late-E bursts. *A*: the 2 *bottom traces* show integrated activities of PN (red) and AbN (black) nerves; the 2nd trace shows raw activity of the RTN/pFRG neuron, and the *top trace* shows the corresponding spike-frequency histogram of this neuron activity (bin = 0.1 s). Note that the neuronal bursts were skipped whenever AbN bursts were skipped, reflecting their synchrony. *B*: interdependence between the RTN/pFRG neuron discharges (shown in *A*) and AbN late-E bursts. Integrated activities of AbN and RTN/pFRG neuron are shown in arbitrary units (a. u.) during a 300 s epoch with sampling frequency of 100 Hz (30,000 points in total) and plotted against each other (red crosses). Dashed lines representing thresholds split the space into 4 quadrants. The top right quadrant represents cases where both cell activity and AbN late-E bursts were present (indicated by blue dashed ellipse); the bottom left quadrant represents cases where both cell and AbN late-E discharges were missing (indicated by another blue dashed ellipse) and only background activity is represented.

Accordingly, we have included in the model a CO_2-sensitive, rhythmically bursting population of neurons in the RTN/pFRG that is postulated to represent a source of late-E AbN bursting.

Dependence of late-E AbN bursting on persistent sodium current (I_{NaP})

Recent modeling studies (Abdala et al. 2009a; Wittmeier et al. 2008) have suggested an intrinsic, cellular, I_{NaP}-dependent mechanism for RTN/pFRG bursting. This previous suggestion is consistent with recent observations in the embryonic parafacial neuronal population (e-pF) that the I_{NaP} blocker, riluzole abolishes rhythmic e-pF neuron activity (Fortin and Thoby-Brisson 2009; Thoby-Brisson et al. 2009). Our new experiments ($n = 5$), illustrated in Fig. 4, *A3* and *B* (right part of the plot), show that riluzole (5 μM in the experiment shown) abolished the AbN late-E activity evoked by hypercapnia (10% CO_2) in the juvenile rat in situ. Although we cannot fully exclude a nonspecific effect of riluzole on general neuronal excitability, these results support the suggestion that population bursting activity in the RTN/pFRG involves endogenous I_{NaP}-dependent bursting properties. It is important to note that the administration of riluzole in these experiments (5–10 μM) suppressed the AbN late-E activity but did not abolish rhythmic respiratory activity although the amplitudes of all motor discharges were reduced (Fig. 4*A3*) as noted previously (Smith et al. 2007). This is fully consistent with our previous in vivo and in situ studies (Paton et al. 2006; Rybak et al. 2007; Smith et al. 2007), showing that respiratory rhythm generation in the intact brain stem under normal conditions is not critically dependent on I_{NaP}.

Late-E activity and temporal relationships between PN and HN discharges

The onset of the PN inspiratory bursts under normal conditions is usually delayed (by ~100 ms) relative to the HN bursts (Fukuda and Honda 1988; Leiter and St.-John 2004; Peever et al. 2002; Rybak et al. 2007; Smith et al. 2007). Interestingly, this delay has been shown to increase during hypercapnia (Fukuda and Honda 1988). In Fig. 5, we show temporal relationships between the onsets of HN and PN bursts during intermittent AbN bursting, extending our original analysis to illustrate in more detail the distributions of delays between HN and PN burst onsets for cases when AbN bursts are present and when they are missed from a representative preparation. The most striking result is that the presence of late-E bursts in the AbN coincides with an increase in the delay between the onsets of HN and the PN bursts (see Fig. 5, *A* and *B*) to ~500 ms (Fig. 5*B*). This suggests that AbN late-E discharge is associated with an enhancement and early onset of HN bursts accompanied by a delay and shortening of PN bursts (see also Abdala et al. 2009a). In our modeling, we incorporate RTN/pFRG interactions with the CPG circuitry that can reproduce these temporal features of the motor outputs.

Patterns of AbN discharge: late-E versus biphasic-E

In contrast to late-E AbN bursting, biphasic-E activity, consisting of pre-I (late-E) and post-I bursts has been recorded from the abdominal motor output in decerebrate neonatal rats (Janczewski and Feldman 2006; Janczewski et al. 2002). This activity pattern is similar to that of single neurons recorded from the RTN/pFRG region of the in vitro isolated brain stem-spinal cord preparation of neonatal rats that show a biphasic-E pattern consisting of a short pre-I discharge and a postinspiratory (rebound) component (Onimaru and Homma 1987, 2006; Onimaru et al. 1988, 1995; see also Wittmeier et al. 2008). The issue of whether the biphasic-E pattern (in both RTN/pFRG and AbN) is a specific characteristic of neonates that transforms to late-E during development or is a characteristic of the specific metabolic conditions of the in vitro preparation (e.g., hypercapnic hypoxia or anoxia) remains unresolved (Abdala et al. 2009a; Ballanyi et al. 1999; Fortuna et al. 2008; Guyenet and Mulkey 2010; Smith et al. 2000; Wittmeier et al. 2008). In the in situ preparations AbN biphasic-E activity was more readily evoked in neonates than in juvenile animals (Abdala et al. 2009a). We have found that in more mature animals transient biphasic-E discharges can be evoked under specific conditions, including hypercapnic anoxia (7% CO_2-93% N_2) or recovery from anoxia-induced central apnea. Similar observations were made by Schwarzacher et al. (1991). In the analysis shown in Fig. 6, we illustrate the consistent finding that transformation of the AbN late-E bursting to a biphasic-E

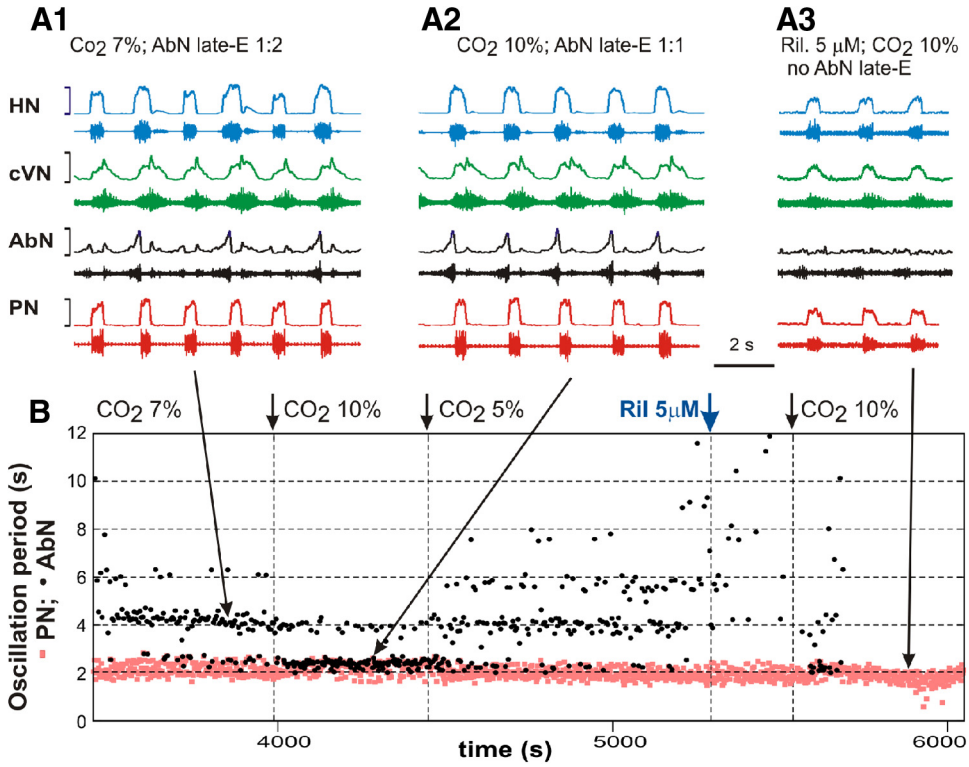

FIG. 4. Effect of riluzole on the hypercapnia-induced AbN late-E activity. *A, 1–3*: simultaneously recoded activity of (bottom-up) PN (red), AbN (black), cVN (green), and HN (blue) nerves. *B*: representation of the entire experimental epoch by plotting the oscillation periods in PN (red squares) and AbN (black circles) vs. time. *A, 1* and *2*, and the corresponding parts of the diagram in *B* (indicated by large arrows) show quantal acceleration of the AbN late-E activity with the development of hypercapnia from 7% CO_2 (see in *B, left,* and *A1* showing a 1:2 ratio between AbN and PN frequencies) to 10% CO_2 (see in *B* after 1st small arrow indicating changing CO_2 to 10% and in *A2* where the ratio of frequencies is 1:1). The level of CO_2 then was returned back to 5% (see 2nd small arrow in *B*) and the frequency of AbN started quantally reducing. Then riluzole (5 μM), the persistent sodium current blocker, was added to the pefusate (indicated in *B* by blue arrow). The right arrow in *B* indicates the moment when CO_2 was increased to 10% in the presence of riluzole. *A3* and *B, right,* shows that riluzole abolished the hypercapnia-evoked AbN late-E activity while only reducing the amplitude (and frequency) of discharges in other nerves.

bursting pattern during hypercapnic anoxia is accompanied by a corresponding reduction/suppression of post-I activity recorded in the cVN. Thus lack of post-I activity appears essential for the expression of the post-I component of the biphasic-E AbN discharge pattern.

Extended model description and validation

The experimental findings described in the preceding text provide the necessary prerequisites for extending our large-scale computational model of the brain stem respiratory network (Smith et al. 2007). This model describes interactions between the respiratory neuron populations spatially organized within brain stem compartments (Fig. 7*A*). The brain stem populations include (right-to-left): a bulbospinal premotor expiratory (bulbospinal E or bs-E) population of the caudal ventral respiratory group (cVRG); a ramp-inspiratory (ramp-I) population of premotor bulbospinal inspiratory neurons and an inhibitory early-inspiratory [early-I(2)] population located in the rostral ventral respiratory group (rVRG); a preinspiratory/inspiratory (pre-I/I) population and inhibitory an early-inspiratory [early-I(1)] population of the pre-BötC; inhibitory augmenting-expiratory (aug-E) and postinspiratory (post-I) populations and an excitatory premotor post-I(e) population in the Bötzinger complex (BötC), and a late-E population representing pFRG and located in RTN/pFRG. The latter population along with the bs-E population represents an extension (and the only difference) in the current model structure (Fig. 7*A*) relative to the model described in Smith et al. (2007). The BötC and pre-BötC populations represent together the core circuitry of the respiratory CPG. In addition, multiple drives from other brain stem components, including the pons, RTN/pFRG and raphé nuclei, provide inputs that regulate the dynamic behavior of this core circuitry as well as activity of premotor neuron populations in the rVRG and cVRG and motor outputs.

The bulbospinal-E population of cVRG was included in the model to generate the expiratory motor output. The neurons of this population were described as those in the ramp-I population and contained only a minimal set of ionic currents necessary for spiking activity. The late-E population of RTN/pFRG was described as the pre-I/I-population and consisted of neurons containing I_{NaP} and having mutual excitatory interactions within the population. The kinetics of I_{NaP} activation in all neurons was based on experimental measurements from acutely dissociated neurons from pre-BötC voltage clamped in vitro (Rybak et al. 2003b; see also Rybak et al. 2007; Smith et al. 2007). The inclusion of this population in the RTN/pFRG compartment and the incorporation I_{NaP} in its neurons were based on the experimental observations described in the preceding text (Figs. 2–4) suggesting that AbN late-E bursting activity originates in the RTN/pFRG and that its generation is critically dependent on I_{NaP}.

Previous theoretical studies have demonstrated that such a population with an I_{NaP}-dependent busting mechanism can operate in the population-bursting mode (at lower excitability or drive) and in the regime of asynchronous sustained activity (when the excitability exceeds a certain threshold) (Butera et al. 1999; Rybak et al. 2003b). Importantly, although the pre-I/I and late-E populations were identical in the model, their behavior was different because of the different excitability of these populations. Specifically, under normal conditions, the pre-I/I population received a strong total excitatory drive from the pons, RTN, and raphé that kept this population in the state of sustained activity independent of I_{NaP} until phasic external inhibition terminated its activity (see Rybak et al. 2003b, 2007; Smith et al. 2007). In contrast, a relatively weak "hypercapnic" drive could evoke I_{NaP}-dependent bursting in the late-E population.

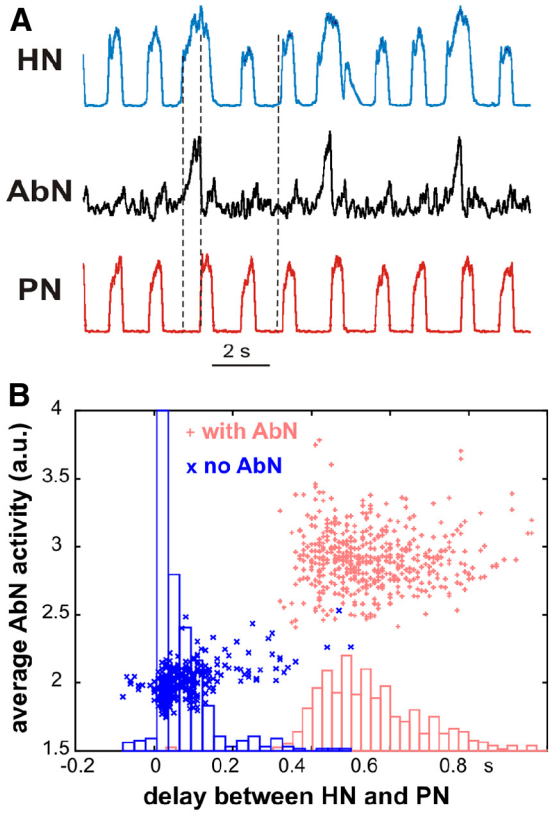

FIG. 5. Effect of late-E activity on the temporal relationships between PN and HN bursts. *A*: integrated activities of PN (*bottom trace,* red), AbN (*middle trace,* black), and HN (*top trace,* blue) nerves during hypercapnic (7% CO_2) regime corresponding to a 1:3 ratio between AbN and PN frequencies. The delay between onsets of PN and HN bursts is substantially longer when late-E bursts are present in AbN than when they are missing (shown by dashed vertical lines). The earlier onset of HN discharges coincides with AbN late-E bursts and the delayed onset of PN bursts coincides with the termination AbN late-E discharges. *B*: the delays between onsets of HN and PN bursts are indicated by small red pluses in the presence of AbN activity and by small blue crosses in the absence of AbN bursts. The corresponding histograms show the distributions of delays between HN and PN onsets for the 2 cases, when AbN bursts are present (red) and when they are missed (blue).

The following connections between the late-E population and other neural populations were incorporated in the model (Fig. 7*A*). *1*) Excitatory connections from the late-E population to the excitatory pre-I/I population of pre-BötC, allowing entrainment of the pre-BötC oscillations by the late-E oscillations. *2*) Inhibitory connections from the inhibitory inspiratory population [early-I(1) of pre-BötC] to the late-E to provide inhibition of late-E neurons during inspiration (Fig. 7*A*). These connections, as well as the connections described above, have been suggested in many previous experimental and modeling studies (Abdala et al. 2009a; Ballanyi et al. 1999; Feldman and Del Negro 2006; Janczewski and Feldman 2006; Janczewski et al. 2002; Joseph and Butera 2005; Onimaru and Homma 1987, 2003; Onimaru et al. 1988, 1995, 2006; Wittmeier et al. 2008). *3*) Excitatory connections from the late-E to the AbN motor output (see Fig. 7*A*), which was based on the previous suggestions (Feldman and Del Negro 2006; Janczewski and Feldman 2006; Janczewski et al. 2002) and our results with local inhibition suggesting that late-E AbN activity originates in the RTN/pFRG. *4*) Excitatory connections from the late-E to the inhibitory populations aug-E (of BötC) and early-I(2) (of rVRG), which both inhibit the premotor ramp-I population (see Fig. 7*A*). These connections were hypothesized to produce an additional delay in the onset of PN discharge by the preceding late-E burst shown in our analysis (Fig. 5). *5*) Inhibitory connections from the post-I population of BötC to the late-E population. These connections were necessary to reproduce the experimental observations described in the sections "*Emergence and quantal acceleration of late-E abdominal activity with hypercapnia*" and "*Patterns of AbN discharge: late-E versus biphasic-E*". The existence of these connections represents one of the key hypotheses of this study.

The performance of the model under simulated normal metabolic conditions (i.e., when the late-E population in the RTN/pFRG is not active) is shown in Fig. 7, *B–D; B* shows the integrated activities of key respiratory populations, *C* exhibits the traces of membrane potential of the corresponding single respiratory neurons (randomly selected from each population), and *D* shows the dynamics of motor outputs (PN, cVN, and HN). The model generates the three-phase eupneic-like respiratory pattern similar to that observed in the in situ preparations under normal conditions. The respiratory oscillations in the model emerge within the BötC/pre-BötC core circuitry due to dynamic interactions among the excitatory neural population in pre-BötC active during inspiration (pre-I/I), the inhibitory population in pre-BötC that provides inspiratory inhibition within the network (early-I(1) of pre-BötC), and the inhibitory populations in the BötC generating expiratory inhibition (post-I and aug-E).

The performance of the model under specific metabolic conditions when the late-E population is active is described in the following sections. Our simulations focused on the three critical behaviors: emergence and quantal acceleration of abdominal late-E activity during hypercapnia, transformation of the late-E bursts to a biphasic-E activity during hypercapnic hypoxia or anoxia, and quantal slowing of BötC/pre-BötC and

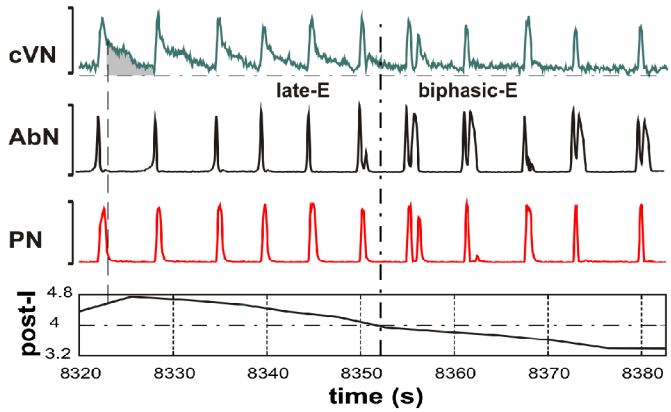

FIG. 6. Transformation of the pattern of abdominal activity from late-E (pre-I) bursting to biphasic-E discharge during hypercapnic anoxia (7% CO_2, 93% N_2). The *top 3 traces* show integrated activity of cVN, AbN, and PN nerves. The *bottom trace* represents the index of postinspiratory (post-I) activity calculated as an averaged activity in cVN during the expiratory phase in each cycle (shown as the gray area in the cVN trace); the expiratory phase was defined by the PN trace (vertical dashed line indicates the onset of expiration). In the 1st half of the recorded episode, only late-E bursts were present in AbN. The post-I component of cVN was progressively reducing. The transition of AbN bursts to a biphasic-E discharge pattern (with pre-I and post-I components) occurred after a significant suppression of the cVN post-I activity (indicated by vertical and horizontal dash-dotted lines).

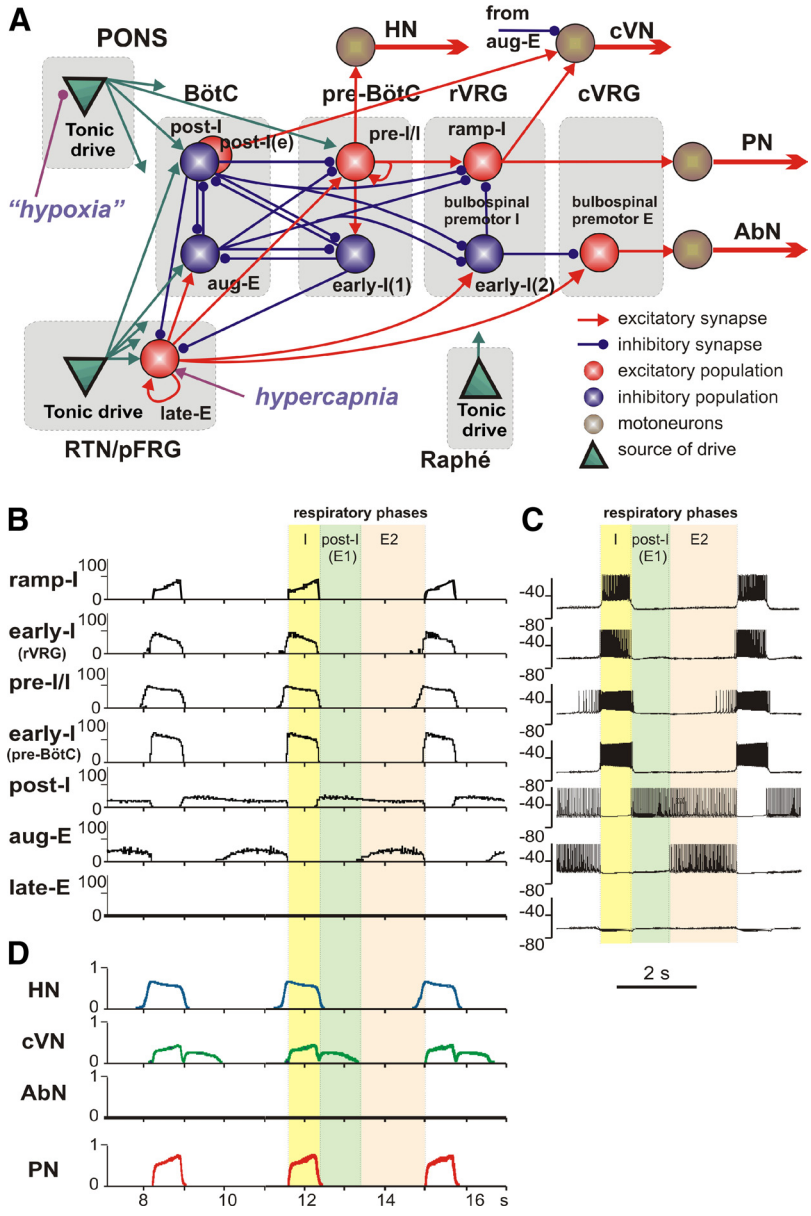

FIG. 7. The extended model of the brain stem respiratory network. *A*: schematic of the extended model showing interactions between different populations of respiratory neurons within major brain stem compartments involved in the control of breathing (pons, RTN/pFRG, BötC, pre-BötC, rVRG, and cVRG). Each population (shown as a sphere) consists of 50 single-compartment neurons described in the Hodgkin-Huxley style. In comparison with the previous model (Smith et al. 2007), this model additionally incorporates the population of bulbospinal premotor expiratory (E) neurons in cVRG, representing the source of AbN activity, and the late-E population in the RTN/pFRG compartment (see text for details), serving as a source of RTN/pFRG oscillations. Justification for all interconnections used in the basic models can be found (with the corresponding references) in our previous papers (Rubin et al. 2009; Rybak et al. 2007; Smith et al. 2007). Justification of interconnections involving the late-E population is in the text. The model includes 3 sources of tonic excitatory drive: pons, RTN, and raphé—all shown as green triangles. These drives, especially those from the pontine and RTN sources project to multiple neural populations in the model (green arrows). However, to simplify the schematic, only the most important connections are shown connected to particular populations. The full structure of connections from each drive source [drive(pons); drive(RTN); drive(raphé)] to target neural populations of the model and the corresponding synaptic weights can be found in Table 1. The late-E population receives an additional external drive simulating the effect of hypercapnia; the pontine drive is considered to be hypoxia/anoxia dependent and was reduced in simulation of hypoxic conditions. *B*: model performance under normal conditions. The activity of major neural populations in the model are represented by average histograms of activity of all neurons in each population (bin = 30 ms). The shown populations include (top-down): ramp-inspiratory (ramp-I located in rVRG), early-inspiratory [early-I(2) in rVRG], preinspiratory/inspiratory (pre-I/I in pre-BötC), early-inspiratory [early-I(1) in pre-BötC], postinspiratory (post-I in BötC), augmenting expiratory (aug-E in BötC), and late-expiratory (late-E in RTN/pFRG). The latter population is silent under normal conditions. *C*: traces of membrane potentials of the corresponding single neurons (randomly selected from each population). *D*: the dynamics of the model's motor outputs: HN (blue); cVN (green); AbN (black, silent under normal conditions); PN (red). In *B–D*, the 3 phase of respiratory cycle are highlighted: inspiratory (I, yellow), postinspiratory (post-I or E1, light green), second expiratory (E2, pink). It is seen that pre-I/I neurons and HN start firing in advance of the beginning of inspiration defined by the onset of PN (and the ramp-I population).

PN oscillations with the progressive suppression of the BötC excitability.

Emergence and quantal acceleration of late-E abdominal activity during hypercapnia

In our model, the late-E population in RTN/pFRG is considered a population of central chemoreceptors the excitability of which is most sensitive to hypercapnia (an increase in the level of CO_2 in the brain stem). The behavior of the model during hypercapnia is shown in Fig. 8. The progressive hypercapnia was simulated as a linear increase of a "hypercapnic" excitatory drive to the late-E population (see Figs. 7*A* and 8, *A, 1–3,* and *B*). The behavior of late-E neurons depends on their intrinsic properties, namely on the voltage-dependent dynamics of I_{NaP} activation and slow inactivation, the phasic inhibition that these neurons receive from the post-I population of BötC during expiration and from the early-I(1) population of pre-BötC during inspiration, and the hypercapnic excitatory drive. As a result, the late-E population begins generating bursts when hypercapnic drive exceeds some threshold (see Fig. 8*B*), which is mostly defined by the post-I inhibition. This post-I inhibition (being reduced during expiration) allows the late-E bursts to appear only close to the end of expiration. The post-I inhibition of late-E together with late-E excitation of pre-BötC pre-I/I neurons provide coupling of RTN/pFRG (late-E) and BötC/pre-BötC oscillations.

Similar to the experimental results with progressive hypercapnia (Figs. 1 and 4) (also Iizuka and Fregosi 2007), the progressive increase of hypercapnic drive in the model evokes quantal acceleration, i.e., step-wise increase in AbN burst frequency with a ratio to PN burst frequency sequentially jumping from 1:4 to 1:3, then to 1:2 and, finally, to 1:1 (see Fig. 8, *A, 1–3,* and *B,* and compare with Fig. 1, *A, 2–4,* and *B*). Figure 8*C* shows the activity of a single pre-I/I neuron of pre-BötC and a single late-E neuron of RTN/pFRG when the ratio of late-E:pre-I/I discharge frequencies is equal to 1:2.

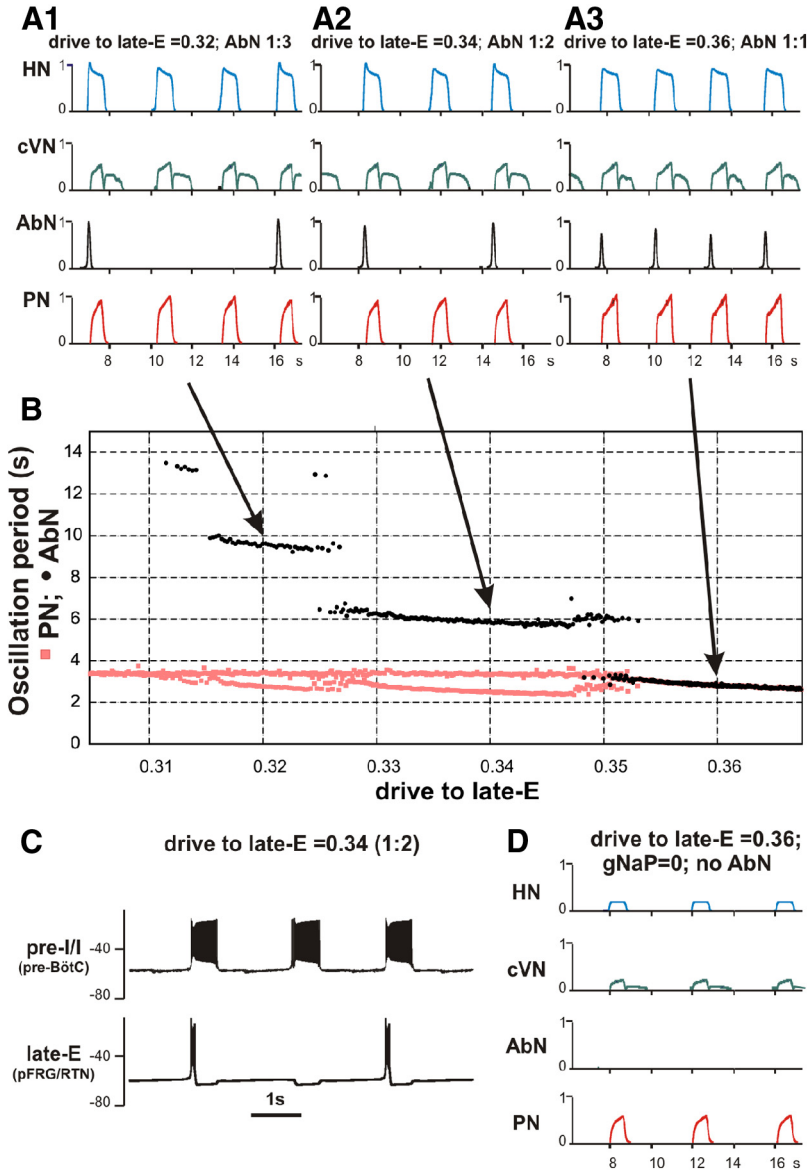

FIG. 8. Modeling the effects of progressive hypercapnia and I_{NaP} blockade. *A, 1–3*: the activity of motor outputs in the model during simulated hypercapnia. The late-E bursts in the AbN were always phase-locked with PN bursts and the ratio between AbN and PN frequencies quantally increased through 1:3 (*A1*) to 1:2 (*A2*) and to 1:1 (*A3*) as "hypercapnic" drive to the late-E population of RTN/pFRG gradually increased to simulate progressive hypercapnia. *B*: the dependence of oscillation periods in AbN (black circles) and PN (red squares) on the hypercapnic drive (horizontal axis). This simulation shows a quantal acceleration of AbN activity during a gradual increase in the simulated hypercapnic drive. The ratio between AbN and PN frequencies sequentially jumped from 1:4 to 1:3 (as in *A1*), then to 1:2 (as in *A2*), and finally to 1:1 (as in *A3*). See Fig. 1 for comparison. With quantal acceleration of AbN activity (after it emerges at 0.31 and before it reaches 1:1 ratio at 0.35) PN periods alternate between 2 red branches depending on the presence or absence of an AbN burst during corresponding breathing cycle. *C*: membrane potential traces of single neurons from the pre-I/I population of pre-BötC (*bottom trace*) and the late-E population of RTN/pFRG (*top trace*) corresponding to the regime of 1:2 coupling between AbN and PN bursts (*A2*). *D*: simulation of the effect of I_{NaP} blockade. Model output motor activities shown correspond to the regime of 1:1 coupling shown in *A3*. The blockade of I_{NaP} was simulated by setting its maximal conductance to 0 in all neurons of the model. This led to a full suppression of AbN activity and a reduction in amplitude and frequency of other simulated motor outputs (compare with Fig. 4*A3*).

Figure 8*D* shows the result of modeling of the effect of riluzole, the I_{NaP} blocker, on the system behavior during hypercapnia. The effect of riluzole was simulated by reducing the I_{NaP} maximal conductance to zero in all neurons of the network (late-E and pre-I/I). Similar to our experimental finding (Fig. 5), the suppression of I_{NaP} during hypercapnia (1:1 coupling regime) fully silenced the late-E AbN (and RTN/pFRG late-E neuron) activity but did not abolish BötC/pre-BötC and PN oscillations. This reflects the differences in tonic drive and hence level of excitation of the late-E versus the pre-I/I neuron populations as described earlier.

Our simulations also show that the late-E bursts when present delay the onset of PN activity and increase the delay between the onsets of HN and PN bursts (Fig. 9). This delay in the model results from an advanced activation of pre-I/I population (projecting to the HN output) by the late-E burst and an additional inhibition of the ramp-I population (projecting to the PN output) by the early-I(2) and aug-E populations excited by the late-E (see Fig. 7*A*). These simulation results are fully consistent with the experimental data described in the preceding text (Fig. 5) and previously by Abdala et al. (2009a).

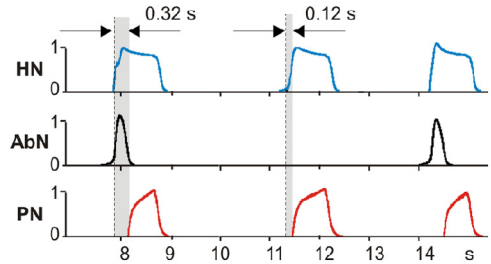

FIG. 9. The effect of late-E activity on the delay between onsets of HN and PN bursts in the model. Three motor outputs of the model are shown (HN, blue; AbN, black; and PN, red) during the hypercapnic regime corresponding to 1:2 ratio between AbN and PN frequencies. The late-E bursts when present increased the delay between onsets of the corresponding HN and PN bursts (indicated by gray bars).

Transformation of the late-E to a biphasic-E activity

As shown in Fig. 6, transformation of AbN late-E bursts to a biphasic-E activity is accompanied by a reduction of the post-I activity. Such a reduction of the post-I activity has been also observed during strong hypoxia or anoxia. As shown previously, the expression of post-I activity strongly depends on pontine input (Dutschmann and Herbert 2006; Rybak et al. 2004). Based on these observations, we suggest that metabolic conditions similar to hypercapnic anoxia can be simulated with our model by applying the "hypercapnic" drive to the late-E population and progressive reduction of the pontine drive to the network (see Fig. 7*A*).

The results of these simulations are shown in Fig. 10*A*. In the simulation shown, the value of drive to the late-E population was initially set to produce 1:1 coupling between late-E and PN activities. Then the pontine drive was progressively reduced from the initial value to zero (Fig. 10*A, bottom trace*). As seen in Fig. 10*A,* reducing the pontine drive produced significant changes in network dynamics. Specifically the post-I component in the cVN output was progressively reduced and the pattern of AbN activity changed from the late-E to a biphasic-E pattern, consisting of a short late-E (pre-I) burst and a stronger postinhibitory rebound. The results of this simulation qualitatively reproduce the experimental results shown in Fig. 6, including the generation of biphasic PN and cVN discharges during the transitional stage. Interestingly, the transformation from the late-E to a biphasic-E pattern in our simulation went through an intermediate stage in which the AbN (and late-E population) activity exhibited only post-I activity without the late-E (pre-I) burst. Figure 10, *B–D,* shows the activity of a single pre-I/I neuron of pre-BötC and a single late-E neuron of RTN/pFRG for all three regimes described.

Quantal slowing of the BötC/pre-BötC and PN activities

The quantal slowing of the pre-BötC and/or PN oscillations has been previously demonstrated with administration of opioid agonists in the in vitro isolated brain stem-spinal cord preparation and in vivo (Janczewski and Feldman 2006; Janczewski et al. 2002; Mellen et al. 2003). Previous attempts to simulate this effect were made by several groups (Abdala et al. 2009a; Joseph and Butera 2005; Wittmeier et al. 2008).

This quantal slowing consists of a step-wise reduction in the frequency of pre-BötC (and/or PN) oscillations resulting from deletion (missing) of a single or a series of inspiratory bursts in the output activity recorded. Although the exact pharmacological effect of opioids is unknown, the general assumption has been that opioids reduce the excitability of pre-BötC neurons either directly or indirectly (via the suppression of excitatory synaptic transmission within the pre-BötC).

To simulate quantal slowing with our model, we first set the hypercapnic drive to the late-E population to produce 1:1 coupling between AbN late-E and PN bursts and then reduced the pontine drive to zero. As a result, both the late-E population and the AbN output in the model exhibited the biphasic-E activity profile with 1:1 coupling to the inspiratory bursts in the pre-BötC and PN (see Fig. 11, *A* and *B,* left parts in both panels).

To produce quantal slowing, the excitatory synaptic conductances within the pre-BötC [in both pre-I and early-I(1) populations] were scaled by a linearly decreasing control function (see Fig. 11*A, bottom trace*). With the gradual decrease of these conductances, the simulated period of BötC/pre-BötC (and PN) oscillations increased in a step-wise manner (see Fig. 11*B*) until these oscillations completely stopped. The frequency of PN (and BötC) oscillations correspondingly de-

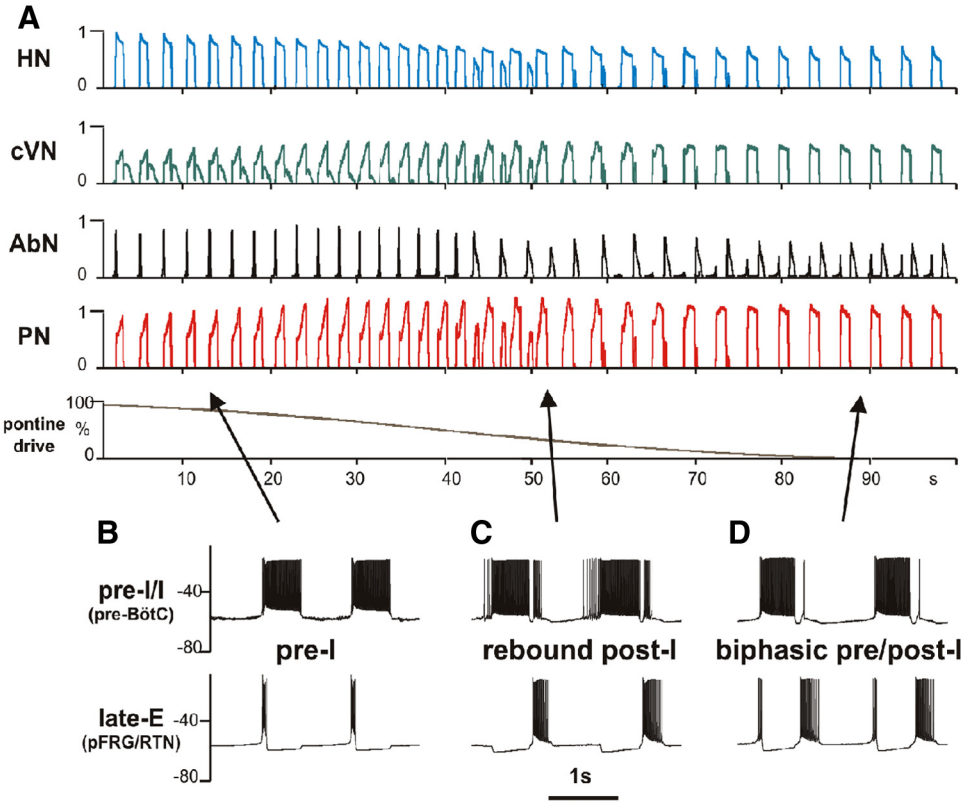

FIG. 10. Transformation of the late-E to a biphasic-E activity with the development of simulated hypoxia. *A*: in this simulation, the value of drive to the late-E population was set to 0.36 to produce 1:1 coupling between the late-E and PN activities (see Fig. 8*A3*). A gradual reduction of pontine drive (*bottom trace*) was used to produce a progressive reduction of post-I activity during development of hypoxia/anoxia (see cVN trace). During this reduction of pontine drive, the AbN pattern sequentially transformed from late-E (pre-I) bursting (see 0–40 s) to a rebound post-I type bursting pattern (40–70 s) and then to a biphasic-E pattern (with pre-I and post-I components (70–100 s). *B–D*: membrane potential traces of single neurons from the pre-I/I population of pre-BötC (*bottom traces*) and the late-E population of RTN/pFRG (*top traces*) corresponding to the AbN late-E (pre-I) pattern (*B*), post-I pattern (*C*) and the biphasic-E pattern (*D*), indicated by arrows.

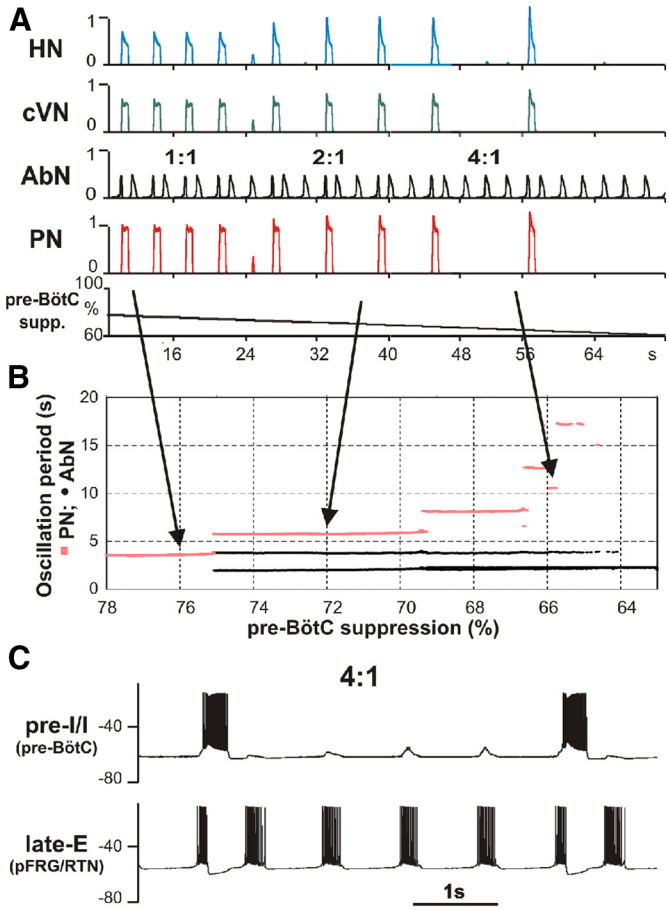

FIG. 11. Simulation of quantal slowing of PN activity. *A*: to simulate quantal slowing of PN activity, we 1st set the value of drive to late-E to 0.36 and the value of pontine drive to 0. This regime corresponded to the end of the simulation shown in Fig. 10 with a biphasic-E pattern of AbN activity. Then the excitability of the pre-BötC neurons [in both the pre-I/I and early-I(1) populations] was linearly decreased by a proportional reduction of all weights of excitatory synapses to pre-I/I and early-I(1) neurons ("pre-BötC suppression," see *lower trace,* starting with 78% of the basic value and reducing this to 0). During progressive reduction of pre-BötC neuronal excitability, the frequency of PN (and HN and cVN) bursts was quantally reduced with the ratio to AbN frequency jumping from 1:1 to 1:2 and so on (see red steps in *B*) until the activity of all nerves except AbN was abolished. *B*: this diagram demonstrates a step-wise dependence of AbN (black circles) and PN (red squares) periods on the pre-BötC's synaptic depression. After the 1st step in PN period (around 75% of normal synaptic weights), 2 different periods of AbN activity were observed. The longer periods correspond to AbN cycles accompanied by PN bursts and the shorter periods correspond to AbN oscillations with PN silent. *C*: membrane potential traces of single neurons from the pre-I/I population of pre-BötC (*bottom traces*) and the late-E population of RTN/pFRG (*top traces*), corresponding to the regime 4:1. Note that the profile of AbN bursts in *A* and late-E bursts in *C* changed from the biphasic-E activity to a monophasic burst whenever the PN bursts were missing.

creased so that the ratio between late-E and PN oscillation frequencies sequentially jumped from 1:1 to 2:1, and then to 4:1, until the full termination of PN bursting.

As mentioned in "*Extended model description and validation",* the pre-I/I population of the pre-BötC consists of neurons with I_{NaP}-dependent bursting properties and mutually excitatory connections. In the regime of quantal slowing, with the reducing neuronal excitability resulting from a decrease in excitatory synaptic conductances, the behavior of this population switches sequentially from a sustained activity to a bursting regime with burst frequency reducing with decreasing neuronal excitability and then to a silent state (see Butera et al. 1999; Rybak et al. 2003b). If isolated from late-E input, the pre-I/I population of pre-BötC would express bursting activity with a very low frequency (and a long interburst recovery period) or would be silent. Therefore in this regime, the excitatory input from the RTN/pFRG late-E population completely controls the timing of pre-I/I (and PN) bursts. The behavior of the model in this regime exactly corresponds to the descriptions provided by Mellen et al. (2003) and Janczewski and Feldman (2006) and to other models (Joseph and Butera 2005; Wittmeier et al. 2008). The RTN/pFRG oscillations are dominant in this case and fully control the timing of pre-BötC (and PN) bursts. This is completely opposite to the regime of quantal acceleration, in which BötC/pre-BötC oscillator dominates and controls the timing of RTN/pFRG bursts.

It is important to note that during deletions of pre-I/I (and PN) bursts the rhythmic activity in the late-E population of RTN/pFRG and in AbN persists, but the profile of their bursts changes from the biphasic-E to a monophasic burst whenever the PN burst is missing (Fig. 11*A*). This is also seen in the activities of single pre-I/I and late-E neurons shown in Fig. 11*C*. These modeling results are consistent with the previously published experimental data (Janczewski and Feldman 2006; Janczewski et al. 2002; Mellen et al. 2003).

Suppression of RTN/pFRG oscillations by inhibition and release by disinhibition

As noted in the preceding text, our model suggests that during normal conditions the BötC/pre-BötC kernel inhibits RTN/pFRG oscillations. Therefore we predict that blocking of inhibitory transmission within RTN/pFRG should evoke (release) oscillations in the RTN/pFRG and AbN at normal metabolic conditions. To investigate this possibility with the model, we kept a small (subthreshold) drive to the late-E population and set to zero the weights of inhibitory connections from BötC/pre-BötC [from both early-I(1) and pos-I populations] to late-E population in RTN/pFRG. The result of this simulation is shown in Fig. 12*A*: the suppression of inhibition to the late-E population evoked bursting activity in both the RTN/pRFG late-E population (not shown) and in AbN. As soon as the inhibition was restored the AbN activity disappeared (Fig. 12*A*).

To verify this prediction experimentally, a small experimental series (on 2 juvenile rat in situ perfused preparations) was performed. In these experiments, $GABA_A$ergic synaptic transmission was blocked/attenuated bilaterally within the ventrolateral (vl) RTN/pFRG by microinjection of the $GABA_A$ antagonist bicuculline (10 μM) under normal metabolic conditions (5% CO_2). In both experiments, microinjection of bicuculline evoked a low-amplitude late-E activity, which then disappeared with washout. The results of one experiment are shown in Fig. 12, *B* and *C,* which are qualitatively similar to our simulation (Fig. 12*A*). These results are consistent with the previously published data showing that RTN/pFRG oscillations can be produced by RTN/pFRG disinhibition (Pagliardini et al. 2009).

DISCUSSION

This study was based on and actually promotes the concept that the kernel of the respiratory CPG resides in the pre-

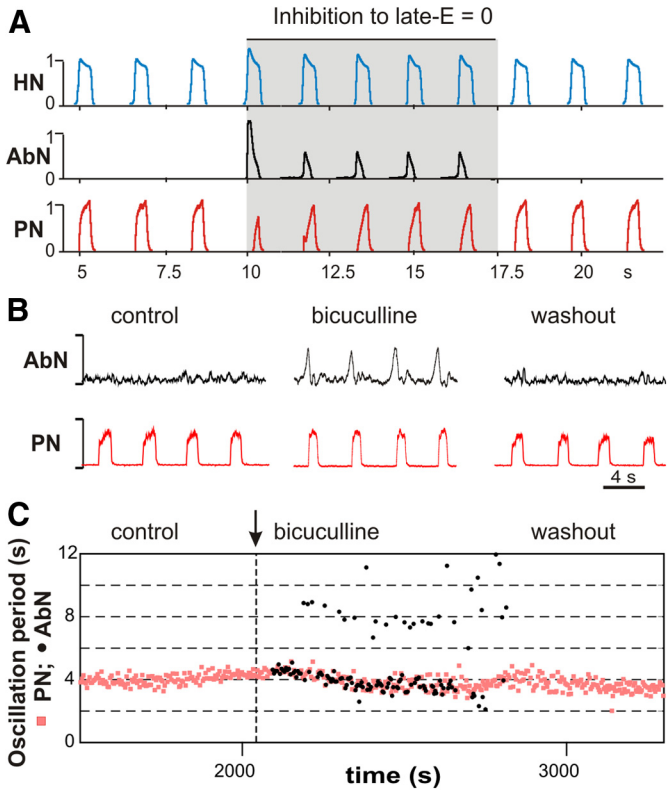

FIG. 12. Release of the AbN late-E busting under normal conditions by suppressing inhibition in RTN/pFRG. *A*: simulation results. The traces of motor outputs PN, AbN and HN generated by the model are shown. Drive to late-E was set to 0.3, below the threshold for late-E population activation (see Fig. 8*B*). To simulate the blockade of inhibition within RTN/pFRG, the weights of inhibitory synapses in late-E neurons were set to 0 during the time interval between 10 and 17.5 s (indicated by gray area). Removing inhibition evoked late-E oscillations in both the late-E population in the RTN/pFRG (not shown) and in the model's AbN output. The bursts generated were phase-locked to PN oscillations. After inhibition returned to the previous level (at 17.5 s), AbN activity disappears. *B* and *C*: experimental testing of the preceding modeling prediction. The experiment shown was performed at normal metabolic conditions with 5% CO_2 in the perfusate. Under control conditions, there was no late-E bursting activity in AbN (see AbN activity in *B, left,* and a lack of black circles in *C* under "control"). Bicuculline (10 μM), a blocker of $GABA_A$ inhibition, was bilaterally microinjected in vl RTN/pFRG at the moment shown in *B* by the vertical dashed line. As seen in *B* (*middle*) and *C* (black circles), the application of bicuculline evoked rhythmic late-E activity in AbN phase-locked with PN bursts. The AbN activity evoked by disinhibition then disappeared with the drug washout (see *B, right,* and lack of black circles in *C, right*).

Bötzinger (pre-BötC) and Bötzinger (BötC) complexes within the medullary ventral respiratory column and that the respiratory rhythm is generated due to dynamic interactions between neural populations within and between these compartments (Abdala et al. 2009a,b; Bianchi et al. 1995; Cohen 1979; Ezure 1990; Ezure et al. 2003; Jiang and Lipski 1990; Richter 1996; Richter and Spyer 2001; Rubin et al. 2009; Rybak et al. 2004, 2007, 2008; Smith et al. 2000, 2007, 2009; Tian et al. 1999).

The other source of respiratory-related oscillations, originally found in the brain stem-spinal cord preparation of the neonatal rat (Onimaru and Homma 1987; Onimaru et al. 1988), was suggested to reside in the RTN/pFRG region and perform the function of an independent generator of preinspiratory/late-expiratory activity (Feldman and Del Negro 2006; Janczewski and Feldman 2006; Janczewski et al. 2002).

In the present study, we performed analyses of experimental data and computational modeling to consider the possible conditions and mechanisms for the emergence of late-expiratory (late-E) oscillations in the RTN/pFRG region and the AbN as well as the possible interactions between the RTN/pFRG oscillations and the respiratory CPG.

Source of late-E oscillations, conditions for their emergence, and the role of I_{NaP}

Experimental data analyzed herein (and in the previous paper by Abdala et al. 2009a) have shown that the high-amplitude late-E activity is not usually expressed in the AbN at the normal metabolic conditions but could be evoked by hypercapnia and other metabolic perturbations (see also Iizuka and Fregosi 2007). We show that the late-E bursts in AbN evoked by hypercapnia (increased CO_2 level) are abolished by pharmacological suppression of the vl RTN/pFRG region (Fig. 2) (see also Abdala et al. 2009a), and we could find single neurons within with RTN/pFRG with hypercapnia-evoked rhythmic activity strongly correlated with the AbN late-E activity (Fig. 3) (see also Abdala et al. 2009a). These findings provide support although indirect for the previous suggestions that the generator of late-E oscillations resides in the RTN/pFRG region and is the source of the AbN late-E activity (Feldman and Del Negro 2006; Janczewski and Feldman 2006; Janczewski et al. 2002).

At the same time, our results (herein and in Abdala et al. 2009a) have clearly demonstrated that late-E oscillations in the AbN (and probably in the RTN/pFRG) are not generated under normal metabolic conditions but emerge during metabolic challenges, such as hypercapnia or hypercapnic hypoxia/anoxia (reduced/removed O_2), at least in the mature animals. Therefore in our opinion, the RTN/pFRG oscillator should not be considered as a fundamental component of the respiratory CPG operating during normocapnia at least in the mature respiratory system. Our data, however, do not allow inferences about a different (e.g., a more dominant or leading) role of the RTN/pFRG oscillations at the embryonic stage or in neonatal animals, which has been widely discussed in the literature (Feldman and Del Negro 2006; Feldman and Janczewski 2006; Feldman et al. 2009; Fortin and Thoby-Brisson 2009; Guyenet et al. 2009; Onimaru et al. 2006; Thoby-Brisson et al. 2009; Wittmeier et al. 2008).

We also showed that the hypercapnia-evoked late-E activity monitored via the AbN was abolished in the mature rat in situ by systemically applied riluzole, an I_{NaP} blocker. The critical role of I_{NaP} in the generation of rhythmic activity in the embryonic parafacial population (e-pF) has been previously demonstrated by administration of riluzole, which abolished the e-pF rhythmic activity (Fortin and Thoby-Brisson 2009; Thoby-Brisson et al. 2009). Our finding is consistent with this data and represents indirect evidence that the generation of rhythmic activity in the RTN/pFRG of the mature animal may also critically depend on I_{NaP}.

Interactions between the RTN/pFRG oscillator and the respiratory CPG

Before discussing the possible connections between the RTN/pFRG oscillator and the core CPG circuitry, we would

like to emphasize the important difference between our concept and model and the dual oscillator concept (Janczewski and Feldman 2006). The latter considers the normal neural machinery for respiratory rhythm and inspiratory pattern generation to reside within the pre-BötC *inspiratory generator*, the rhythmic activity of which is fully defined by the intrinsic (or group-pacemaker) properties and excitatory interconnections within this region. In our opinion, this concept undervalues the role of other brain stem compartments, such as the BötC and pons, and interactions between them (including inhibitory interactions) in the generation of respiratory rhythm and pattern. In contrast, in our concept and the model, the respiratory rhythm is generated because of the dynamic interactions within and between the pre-BötC and BötC, representing the core of the CPG, under control of other brain stem compartments including the pons, RTN, and raphé (Abdala et al. 2009a; Rybak et al. 2004, 2007, 2008; Smith et al. 2007, 2009). Therefore concerning interactions between the RTN/pFRG oscillator and the respiratory CPG, these interactions in our opinion also involve interactions with other critical components of the CPG, including the BötC and rVRG.

A schematic of interactions between the RTN/pFRG oscillator and the respiratory CPG (with BötC/pre-BötC kernel) predicted by our model is shown in Fig. 13. These important interactions include excitation of the BötC/pre-BötC oscillator, specifically the excitatory preinspiratory/inspiratory neurons of the pre-BötC (pre-I/I, see Fig. 7*A*) by the RTN/pFRG oscillations, and inhibition of the RTN/pFRG oscillations by the BötC/pre-BötC oscillator during inspiration by the early-inspiratory population of the pre-BötC [early-I(1), see Fig. 7*A*]. These two interactions have been suggested and justified in many previous experimental and modeling studies (Abdala et al. 2009a; Ballanyi et al. 1999; Feldman and Del Negro 2006; Janczewski and Feldman 2006; Janczewski et al. 2002; Joseph and Butera 2005; Onimaru and Homma 1987, 2003; Onimaru et al. 1988, 1995, 2006; Wittmeier et al. 2008).

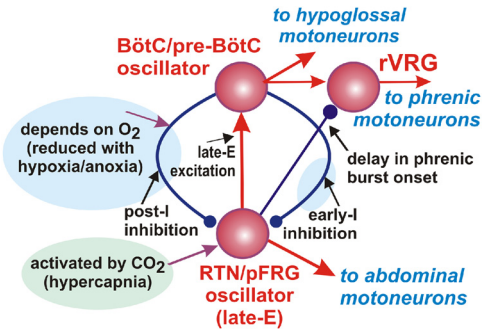

FIG. 13. Proposed interactions between BötC/pre-BötC and RTN/pFRG oscillators in adult mammals in vivo. Red arrows represent excitatory influence; blue lines terminated with circles indicate inhibitory influence; violet arrows indicate metabolic dependence. Under normal metabolic conditions, the RTN/pFRG oscillator is inhibited by the BötC/pre-BötC oscillator (the core of the respiratory CPG) during both inspiration (by the inhibitory early-I neurons of pre-BötC) and expiration (by the post-I neurons of BötC) and remains silent. The normal expression of post-I inhibition requires excitatory drive from the pons (not shown). The RTN/pFRG oscillator can be activated either by hypercapnia, which directly excites RTN/pFRG neurons, or by hypoxia/anoxia (or pontine suppression), which reduces RTN/pFRG inhibition by the BötC/pre-BötC oscillator, or by both. When activated, the RTN/pFRG oscillator provides both excitation of the BötC/pre-BötC oscillator and inhibition of rVRG premotor neurons, hence increasing the delay between hypoglossal and phrenic discharges.

In addition to the above interactions, we hypothesize inhibitory connections (direct or indirect) from the RTN/pFRG to the premotor inspiratory neurons of rVRG (Fig. 13), e.g., via the augmenting-expiratory (aug-E) and/or early-inspiratory [early-I(2)] populations (see Fig. 7*A*). These hypothesized connections provide a reasonable explanation for the additional delay between the HN and PN motor outputs associated with the late-E bursts in the abdominal motor output (Figs. 5 and 9) as well as for an increase of this delay generally observed during hypercapnia (Fukuda and Honda 1988).

The other connection hypothesized in our study is the inhibitory connection from the BötC/pre-BötC kernel (specifically from post-I neurons of the BötC, see Fig. 7*A*) to the RTN/pFRG oscillator (Fig. 13). This connection provides a decreasing inhibition of RTN/pFRG during expiration. Based on our modeling studies, we hypothesize that this connection performs three important functions. First, it significantly contributes to the coupling between RTN/pFRG late-E and pre-BötC bursts by not allowing late-E RTN/pFRG bursting to occur before the end of expiration. Second, this expiratory inhibition together with the inspiratory inhibition (see preceding text) may keep RTN/pFRG oscillations inhibited during normal conditions. Third, this inhibition may suppress the second rebound burst of AbN (and, probably, RTN/pFRG).

Based on the suggested schematic of interactions between the RTN/pFRG and BötC/pre-BötC kernel (Figs. 7*A* and 13), we conclude that RTN/pFRG activity is strongly controlled by BötC/pre-BötC inhibition during both inspiration and expiration; this fits to the general schematic of interactions between RTN and the CPG proposed by the Guyenet group (Guyenet 2008; Guyenet et al. 2005). Moreover, based on our simulation, we suggest that the activity of RTN/pFRG is actually more strongly controlled by the BötC/pre-BötC activity than the activity of BötC/pre-BötC is controlled by RTN/pFRG oscillations. This control of RTN/pFRG activity by the BötC/pre-BötC circuits includes control of the emergence of RTN/pFRG oscillations and of their frequency and coupling to BötC/pre-BötC oscillations, which is clearly demonstrated by the regime of quantal acceleration of late-E activity with the development of hypercapnia (Figs. 1, 4, and 8).

As stated in the preceding text, our model suggests that during normal conditions the BötC/pre-BötC kernel inhibits RTN/pFRG oscillations, and our simulation results demonstrated that blocking of fast inhibitory synaptic transmission within RTN/pFRG in the model should evoke (release) oscillations in the RTN/pFRG and AbN at normal metabolic conditions. We then verified this prediction experimentally, although in our experiments, we cannot fully exclude a possibility that this inhibition of RTN/pFRG is produced by sources other than the BötC post-I population. This issue requires further experimental investigations.

Effects of hypercapnia and hypoxia on RTN/pFRG activity

Our studies (previous and herein) show that the late-E activity in AbN (and probably in RTN/pFRG) is usually not generated under normal metabolic conditions. At the same time, the excitability of the late-E population in RTN/pFRG is highly sensitive to hypercapnia. Therefore the progressive hypercapnia producing depolarization of late-E neurons can overcome the inhibition by BötC/pre-BötC and initiate late-E

rhythmic activity that goes through several stages described herein as quantal acceleration until the late-E activity reaches 1:1 coupling with the BötC/pre-BötC oscillations (see Figs. 1 and 8). In contrast, strong hypoxia or anoxia can affect the RTN/pFRG oscillations through reduction of inhibition, specifically post-I inhibition (see Fig. 13) and produce an effect similar to hypercapnia by shifting a balance between inhibition and excitation at the RTN/pFRG late-E neurons.

In summary, we suggest that the emergence of RTN/pFRG and abdominal (late-E) oscillations is defined by the balance between the two major factors (Fig. 13): general RTN/pFRG excitability, which increases with CO_2 level (hypercapnia), and inhibition of RTN/pFRG oscillator by BötC/pre-BötC circuits during both inspiration (by inspiratory inhibitory neurons of the pre-BötC) and expiration (by the postinspiratory inhibitory neurons of the BötC), which depends on the level of O_2 (hypoxia). Therefore the late-E oscillations in the RTN/pFRG (and in the abdominal motor output) are suppressed under normal metabolic conditions but can emerge with the development of hypercapnia or hypoxia. The same metabolic factors define the profile of RTN/pFRG and abdominal discharges, so that a progressive development of hypoxia under hypercapnic conditions transforms the late-E (pre-I) pattern to a biphasic-E activity with pre-I and post-I components. Alternatively, the RTN/pFRG oscillations when emerge exert a positive (excitatory) influence on the pre-BötC's inspiratory neurons and hypoglossal motor output and a negative (inhibitory) effect on the premotor bulbospinal inspiratory neurons of rVRG and phrenic motor output, hence increasing the delay between the onsets of hypoglossal and phrenic bursts. The latter is likely to provide a necessary state-dependent coordination between control of upper airway, abdominal muscle contraction and lung inflation/deflation during breathing.

Synchronization-based control of the respiratory CPG

As described previously (Abdala et al. 2009a) and herein, the RTN/pFRG oscillations are not generated under normal conditions but emerge and interact with the respiratory CPG under specific metabolic conditions, such as hypercapnia. The effect of these oscillations on the respiratory CPG may be considered as an example of "synchronization-based" control of the respiratory CPG (see INTRODUCTION). Specifically, as shown in the case of hypercapnia, this type of control may operate via periodical or *quantal* effects of RTN/pFRG on the CPG, which can accelerate or slow down depending on the level of CO_2. The results of these studies may have a broader impact on understanding a synchronization-based control in other CPGs.

Extended model and its validation

In this study, we extended and used our previous computational model (Rybak et al. 2007; Smith et al. 2007). The previous model was able to reproduce the three-phase eupneic respiratory pattern generated under normal conditions as well as the reorganization of this pattern caused by multiple experimental perturbations, such as various brain stem transections and application of specific blockers of ionic channels and inhibitory synaptic transmission. It is interesting to note that since the first publications of the basic version of our model (Rubin et al. 2009; Rybak et al. 2007; Smith et al. 2007), several modeling predictions have been (directly or indirectly) confirmed by experimental studies. For example, our model suggested that the pre-BötC compartment should contain a population of inhibitory neurons [early-I(1) in Fig. 7*A*] that provides inspiratory inhibition in the network. In agreement with this suggestion, Winter et al. (2009) have recently found a population of glycinergic inspiratory neurons within the pre-BötC that can "make important contribution to generation and maintenance of the respiratory rhythm." The critical role of inhibitory neurons in the BötC for rhythm generation suggested by our model has been confirmed indirectly by Bongianni et al. (2010). These researchers have demonstrated that blockade of $GABA_A$ receptors in the BötC (of rabbit) by bicuculline or gabazine induces strong depression of respiratory activity up to apnea. These new results provide additional indirect support for the importance of the mutual inhibitory interactions between the BötC and pre-BötC for respiratory rhythm generation as proposed by our previous and extended models.

Morgado-Valle et al. (2010) have recently found in vitro a subpopulation of glycinergic inhibitory neurons with pacemaker-like properties within the pre-BötC. These authors suggest that this finding challenges our network models, which in their opinion critically depend on excitatory pacemaker neurons within the pre-BötC. In this connection, we emphasize that all our previous models (Rubin et al. 2009; Rybak et al. 2004, 2007, 2008; Smith et al. 2007) and the model described herein always included an inhibitory population of pre-BötC neurons [see early-I(1) in Fig. 7], and that the generation of respiratory rhythm in these models under normal conditions is not critically dependent on excitatory pacemaker neuron activity, which was demonstrated with full suppression of I_{NaP} that does not disrupt rhythm generation experimentally and in these models (see Rybak et al. 2007, 2008; Smith et al. 2007) (see also Fig. 8*D*). We suggest that the inhibitory neuron pacemaker properties described by Morgado-Valle et al. (2010) cannot represent a basis for population bursting because such neurons cannot excite each other to generate coherent inspiratory bursting. Moreover, in contrast to other suggestions based on reduced in vitro preparations (e.g., see Del Negro et al. 2009), we propose that the role of intrinsic pacemaker or group-pacemaker mechanisms is significantly reduced in the more intact network under in situ/in vivo conditions, at least in mature animals, and that network interactions as depicted in Fig. 7 play a dominant role in rhythmogenesis per se as well as in the control of phase durations and respiratory pattern expressed by the network.

Our current study focused on the interactions between the BötC/pre-BötC kernel of the CPG and the RTN/pFRG oscillations that emerge under specific metabolic conditions. To study these interactions we extended the previous model by incorporating the late-E population with I_{NaP}-dependent bursting properties in the RTN/pFRG compartment and proposed specific connections between the BötC/pre-BötC kernel and this late-E population generating RTN/pFRG oscillations. These hypothesized connections allow the extended model to reproduce and explain several key behaviors including the emergence and quantal acceleration of abdominal late-E activity during hypercapnia, transformation of the late-E bursts to a biphasic-E activity during hypercapnic hypoxia or anoxia, and quantal slowing of BötC/pre-BötC and PN oscillations with the progressive suppression of pre-BötC excitability. The ability of the extended model to reproduce these behaviors provides

additional validation for the model per se and for the hypothesized interactions between the RTN/pFRG and the respiratory CPG. The proposed interactions and their hypothesized dependence on metabolic conditions require further experimental testing. The current model provides a framework and tool for further experimental and theoretical studies.

We emphasize that the primarily goal of our current modeling studies was to reproduce experimental data on the hypercapnic response, specifically the emergence of RTN/pFRG and late-E motor activity, obtained in the arterially perfused preparation (Abdala et al. 2009a; see Figs. 1–6). We have not tried to reproduce with the current model all the effects of hypercapnia observed in vivo and in various preparations, such as an increase in breathing frequency and/or minute ventilation (breathing frequency multiplied by amplitude of inspiratory activity). It is known that hypercapnia normally augments ventilation that increases with the level of CO_2. Depending on the experimental conditions/preparation used, this hypercapnia-evoked increase in ventilation varies in magnitude and is mediated by an increase in either the respiratory frequency or the amplitude of inspiratory motor activity, or both (Abu-Shaweesh et al. 1999; Iizuka and Fregosi 2007; Li et al. 1999; Strohl et al. 1997; Zhou et al. 1996). The arterially perfused in situ preparation used in our studies (Abdala et al. 2009a) can also demonstrate an increase in inspiratory frequency if CO_2 is raised from 2–3% up to ~5.0–5.5% where it saturates and does not typically respond to further CO_2 increases (see St.-John and Paton 2000). Furthermore, 5% of CO_2 in the perfusate provides a normal arterial CO_2 tension and normal pH in the perfusate and hence is usually considered to be the baseline (normocapnic) conditions in this preparation. At the same time, this level of CO_2 appears to be within the saturation part of the preparation frequency response to CO_2 increase. Hence no obvious frequency increases were observed in the Abdala et al. (2009a) studies when CO_2 was increased above the base level of 5% (see Figs. 1 and 4). This pattern of response appears not to be specific to the in situ preparation as hypercapnia did not evoke an increase in breathing frequency in some experiments performed on artificially ventilated rats in vivo (e.g., Iizuka and Fregosi 2007) although a steep increase in inspiratory amplitude was observed.

In general, changes in CO_2 (and pH) can potentially affect the intrinsic neuronal properties, synaptic and neuromodulatory mechanisms, neuronal activities within, and interactions between, different brain stem compartments (VRC, pons, NTS, RTN, raphé) as well as pathways/properties of peripheral mechanoreceptor and chemoreceptor feedback, all of which are involved (to some degree) in the system's response to hypercapnia. Hence the use of the current computational model for a direct simulation and mechanistic explanation of the system's response to changes in CO_2 cannot be done presently with a reasonable degree of speculation because of the current lack of knowledge. In this regard, our previous (Rubin et al. 2009; Smith et al. 2007) and current models do not explicitly use the concentration of CO_2 (and O_2) or their partial pressure as model parameters. Instead we consider (as model parameters) excitatory drives to each respiratory neural population from several potentially involved sources (pons, RTN, raphé). In our previous study (Rubin et al. 2009), we specifically investigated how changes in these drives and in the total cumulative drive to each population in the model can affect the frequency of the output (phrenic) oscillations. For example, it was shown that an increase in the total drive to the pre-BötC pre-I/I population can produce up to a threefold increase in breathing frequency. Hence we have a mechanistic understanding of how these drives control respiratory frequency, which may be involved in hypercapnic responses, but it is still unknown how specifically the CO_2 level governs each drive from the pons, RTN, and raphé to each particular population of respiratory neurons. While the reproduction of systems-level behaviors including hypercapnia-evoked increases of ventilation has not been a specific task in our present modeling studies, this is an objective of our future experimental and computational studies that will involve further model elaboration. Nevertheless our current model can reproduce and explain the major features of the hypercapnic response in situ involving the emergence of RTN/pFRG and late-E abdominal motor activity.

GRANTS

This study was supported by National Institute of Neurological Disorders and Stroke Grant R01 NS-057815 to I. A. Rybak and in part by the Intramural Research Program of the NIH, NINS funding to J. C. Smith. J.F.R. Paton is the recipient of a Royal Society Wolfson Research Merit Award.

DISCLOSURES

No conflicts of interest, financial or otherwise, are declared by the author(s).

REFERENCES

Abdala AP, Rybak IA, Smith JC, Paton JF. Abdominal expiratory activity in the rat brain stem-spinal cord in situ: patterns, origins and implications for respiratory rhythm generation. *J Physiol* 587: 3539–3559, 2009a.

Abdala AP, Rybak IA, Smith JC, Zoccal DB, Machado BH, St-John WM, Paton JF. Multiple pontomedullary mechanisms of respiratory rhythmogenesis. *Respir Physiol Neurobiol* 168: 19–25, 2009b.

Abu-Shaweesh JM, Dreshaj IA, Thomas AJ, Haxhiu MA, Strohl KP, Martin RJ. Changes in respiratory timing induced by hypercapnia in maturing rats. *J Appl Physiol* 87: 484–490, 1999.

Baker SN, Kilner JM, Pinches EM, Lemon RN. The role of synchrony and oscillations in the motor output. *Exp Brain Res* 128: 109–117, 1999.

Ballanyi K, Onimaru H, Homma I. Respiratory network function in the isolated brainstem-spinal cord of newborn rats. *Prog Neurobiol* 59: 583–634, 1999.

Bauer M, Oostenveld R, Peeters M, Fries P. Tactile spatial attention enhances gamma-band activity in somatosensory cortex and reduces low-frequency activity in parieto-occipital areas. *J Neurosci* 26: 490–501, 2006.

Bazhenov M, Timofeev I, Steriade M, Sejnowski TJ. Self-sustained rhythmic activity in the thalamic reticular nucleus mediated by depolarizing GABAA receptor potentials. *Nat Neurosci* 2: 168–174, 1999.

Bianchi AL, Denavitsaubie M, Champagnat J. Central control of breathing in mammals: neuronal circuitry, membrane properties, and neurotransmitters. *Physiol Rev* 75: 1–45, 1995.

Bongianni F, Mutolo D, Cinelli E, Pantalleo T. Respiratory responses induced by blockades of GABA and glycine receptors within the Bötzinger complex and the pre-Bötzinger complex of the rabbit. *Brain Res* 1344: 134–147, 2010.

Butera RJ, Rinzel JR, Smith JC. Models of respiratory rhythm generation in the pre-Bötzinger complex: II. Populations of coupled pacemaker neurons. *J Neurophysiol* 82: 398–415, 1999.

Cohen MI. Neurogenesis of respiratory rhythm in the mammal. *Physiol Rev* 59: 1105–1173, 1979.

Del Negro CA, Kam K, Hayes JA, Feldman JL. Asymmetric control of inspiratory and expiratory phases by excitability in the respiratory network of neonatal mice in vitro. *J Physiol* 587: 1217–1231, 2009.

Dutschmann M, Herbert H. The Kölliker–Fuse nucleus gates the postinspiratory phase of the respiratory cycle to control inspiratory off-switch and upper airway resistance in rat. *Eur J Neurosci* 24: 1071–1084, 2006.

Elsen FP, Ramirez JM. Calcium currents of rhythmic neurons recorded in the isolated respiratory network of neonatal mice. *J Neurosci* 18: 10652–10662, 1998.

Ezure K. Synaptic connections between medullary respiratory neurons and considerations on the genesis of respiratory rhythm. *Prog Neurobiol* 35: 429–450, 1990.

Ezure K, Tanaka I, Saito Y. Brain stem and spinal projections of augmenting expiratory neurons in the rat. *Neurosci Res* 45: 41–51, 2003.

Feldman JL, Del Negro CA. Looking for inspiration: new perspectives on respiratory rhythm. *Nat Rev Neurosci* 7: 232–242, 2006.

Feldman JL, Janczewski WA. Point:Counterpoint: the parafacial respiratory group (pFRG)/pre-Bötzinger complex (pre-BötC) is the primary site of respiratory rhythm generation in the mammal. Counterpoint: the pre-BötC is the primary site of respiratory rhythm generation in the mammal. *J Appl Physiol* 100: 2096–2097, 2006.

Feldman JL, Kam K, Janczewski WA. Practice makes perfect, even for breathing. *Nat Neurosci* 12: 961–963, 2009.

Fortin G, Thoby-Brisson M. Embryonic emergence of the respiratory rhythm generator. *Respir Physiol Neurobiol* 168: 86–91, 2009.

Fortuna MG, West GH, Stornetta RL, Guyenet PG. Bötzinger expiratory augmenting neurons and the parafacial respiratory group. *J Neurosci* 28: 2506–2515, 2008.

Frermann D, Keller BU, Richter DW. Calcium oscillations in rhythmically active respiratory neurons in the brain stem of the mouse. *J Physiol* 515: 119–131, 1999.

Fukuda Y, Honda Y. Modification by chemical stimuli of temporal difference in the onset of inspiratory activity between vagal (superior laryngeal) or hypoglossal and phrenic nerves of the rat. *Jpn J Physiol* 38: 309–319, 1988.

Grillner S, Markram H, DeSchutter E, Silberberg G, LeBeau FEN. Microcircuits in action: from CPGs to neocortex. *Trends Neurosci* 28: 525–533, 2005.

Guyenet PG. Carl Ludwig Lecture: retrotrapezoid nucleus, CO2 homeostasis, and breathing automaticity. *J Appl Physiol* 105: 404–416, 2008.

Guyenet PG, Bayliss DA, Stornetta RL, Fortuna MG, Abbott SB, DePuy SD. Retrotrapezoid nucleus, respiratory chemosensitivity and breathing automaticity. *Respir Physiol Neurobiol* 168: 59–68, 2009.

Guyenet PG, Mulkey DK. Retrotrapezoid nucleus and parafacial respiratory group. *Respir Physiol Neurobiol* 173: 244–255, 2010.

Guyenet PG, Mulkey DK, Stornetta RL, Bayliss DA. Regulation of ventral surface chemoreceptors by the central respiratory pattern generator. *J Neurosci* 25: 8938–8947, 2005.

Hegger R, Kantz H, Schreiber T. Practical implementation of nonlinear time series methods: The TISEAN package. *Chaos* 9: 413–435, 1999.

Iizuka M, Fregosi RF. Influence of hypercapnic acidosis and hypoxia on abdominal expiratory nerve activity in the rat. *Respir Physiol Neurobiol* 157: 196–205, 2007.

Janczewski WA, Feldman JL. Distinct rhythm generators for inspiration and expiration in the juvenile rat. *J Physiol* 570: 407–420, 2006.

Janczewski WA, Onimaru H, Homma I, Feldman JL. Opioid-resistant respiratory pathway from the preinspiratory neurones to abdominal muscles: *in vivo* and *in vitro* study in the newborn rat *J Physiol* 545: 1017–1026, 2002.

Jiang C, Lipski J. Extensive monosynaptic inhibition of ventral respiratory group neurons by augmenting neurons in the Bötzinger complex in the cat. *Exp Brain Res* 81: 639–648, 1990.

Joseph IM, Butera RJ. A simple model of dynamic interactions between respiratory centers. *Conf Proc IEEE Eng Med Biol Soc* 6: 5840–5842, 2005.

Kay LM, Beshel J, Brea J, Martin C, Rojas-Libano D, Kopell N. Olfactory oscillations: the what, how and what for. *Trends Neurosci* 32: 207–214, 2009.

Koshiya N, Smith JC. Neuronal pacemaker for breathing visualized in vitro. *Nature* 400: 360–363, 1999.

Leiter JC, St. -John WM. Phrenic, vagal and hypoglossal activities in rat: pre-inspiratory, inspiratory, expiratory components. *Respir Physiol Neurobiol* 142: 115–125, 2004.

Li A, Randall M, Nattie EE. CO_2 microdialysis in retrotrapezoid nucleus of the rat increases breathing in wakefulness but not in sleep. *J Appl Physiol* 87: 910–919, 1999.

Marder E, Calabrese RL. Principles of rhythmic motor pattern generation. *Physiol Rev* 76: 687–717, 1996.

Mellen NM, Janczewski WA, Bocchiaro CM, Feldman JL. Opioid-induced quantal slowing reveals dual networks for respiratory rhythm generation. *Neuron* 37: 821–826, 2003.

Morgado-Valle C, Baca SM, Feldman JL. Glycinergic pacemaker neurons in preBötzinger Complex of neonatal mouse. *J Neurosci* 30: 3634–3639, 2010.

Onimaru H, Arata A, Homma I. Primary respiratory rhythm generator in the medulla of brain stem-spinal cord preparation from newborn rat. *Brain Res* 445: 314–324, 1988.

Onimaru H, Arata A, Homma I. Intrinsic burst generation of preinspiratory neurons in the medulla of brain stem-spinal cord preparations isolated from newborn rats. *Exp Brain Res* 106: 57–68, 1995.

Onimaru H, Homma I. Respiratory rhythm generator neurons in medulla of brain stem-spinal cord preparation from newborn rat. *Brain Res* 403: 380–384, 1987.

Onimaru H, Homma I. A novel functional neuron group for respiratory rhythm generation in the ventral medulla. *J Neurosci* 23: 1478–1486, 2003.

Onimaru H, Ikeda K, Kawakami K. Phox2b, RTN/pFRG neurons and respiratory rhythmogenesis. *Respir Physiol Neurobiol* 168: 13–18, 2009.

Onimaru H, Kumagawa Y, Homma I. Respiration-related rhythmic activity in the rostral medulla of newborn rats. *J Neurophysiol* 96: 55–61, 2006.

Pagliardini S, Tan W, Janczewski WA, Feldman JL. Excitation and disinhibition of RTN/pFRG neurons induce active expiration in adult rats. In: *The XI-th Oxford Conference on Modeling and Control of Breathing: New Frontiers in Respiratory Control, Program and Abstracts.* Nara, Japan: 2009, p. 101.

Paton JFR, Abdala APL, Koizumi H, Smith JC, St-John WM. Respiratory rhythm generation during gasping depends on persistent sodium current. *Nat Neurosci* 9: 311–313, 2006.

Peever JH, Shen L, Duffin J. Respiratory pre-motor control of hypoglossal motoneurons in the rat. *Neurosci* 110: 711–712, 2002.

Rekling JC, Feldman JL. PreBötzinger complex and pacemaker neurons: hypothesized site and kernel for respiratory rhythm generation. *Annu Rev Physiol* 60: 385–405, 1998.

Richter DW. Neural regulation of respiration: rhythmogenesis and afferent control. In: *Comprehensive Human Physiology*, edited by Gregor R and Windhorst U. Berlin: Springer-Verlag, 1996, vol. 2, p. 2079–2095.

Richter DW, Spyer KM. Studying rhythmogenesis of breathing: comparison of in vitro and in vivo models. *Trends Neurosci* 24: 464–472, 2001.

Rubin JE, Shevtsova NA, Ermentrout GB, Smith JC, Rybak IA. Multiple rhythmic states in a model of the respiratory central pattern generator. *J Neurophysiol* 101: 2146–2165, 2009.

Rybak IA, Abdala AP, Markin SN, Paton JF, Smith JC. Spatial organization and state-dependent mechanisms for respiratory rhythm and pattern generation. *Prog Brain Res* 165: 201–220, 2007.

Rybak IA, O'Connor R, Ross A, Shevtsova NA, Nuding SC, Segers LS, Shannon R, Dick TE, Dunin-Barkowski WL, Orem JM, Solomon IC, Morris KF, Lindsey BG. Reconfiguration of the pontomedullary respiratory network: a computational modeling study with coordinated in vivo experiments. *J Neurophysiol* 100: 1770–1799, 2008.

Rybak IA, Ptak K, Shevtsova NA, McCrimmon DR. Sodium currents in neurons from the rostroventrolateral medulla of the rat. *J Neurophysiol* 90: 1635–1642, 2003a.

Rybak IA, Shevtsova NA, Paton JF, Dick TE, St-John WM, Morschel M, Dutschmann M. Modeling the ponto-medullary respiratory network. *Respir Physiol Neurobiol* 143: 307–319, 2004.

Rybak IA, Shevtsova NA, St-John WM, Paton JF, Pierrefiche O. Endogenous rhythm generation in the pre-Bötzinger complex and ionic currents: modelling and in vitro studies. *Eur J Neurosci* 18: 239–257, 2003b.

Schwarzacher S, Wilhelm Z, Anders K, Richter D. The medullary respiratory network in the rat. *J Physiol* 435: 631–644, 1991.

Singer W. Synchronization of cortical activity and its putative role in information processing and learning. *Annu Rev Physiol* 55: 349–374, 1993.

Smith JC, Abdala AP, Koizumi H, Rybak IA, Paton JF. Spatial and functional architecture of the mammalian brain stem respiratory network: a hierarchy of three oscillatory mechanisms. *J Neurophysiol* 98: 3370–3387, 2007.

Smith JC, Abdala AP, Rybak IA, Paton JF. Structural and functional architecture of respiratory networks in the mammalian brain stem. *Philos Trans R Soc Lond B* 364: 2577–2587, 2009.

Smith JC, Butera RJ, Koshiya N, Del Negro C, Wilson CG, Johnson SM. Respiratory rhythm generation in neonatal and adult mammals: the hybrid pacemaker-network model. *Respir Physiol* 122: 131–147, 2000.

Smith JC, Ellenberger HH, Ballanyi K, Richter DW, Feldman JL. Pre-Bötzinger complex: a brain stem region that may generate respiratory rhythm in mammals. *Science* 254: 726–729, 1991.

St-John WM, Paton JF. Characterizations of eupnea, apneusis and gasping in a perfused rat preparation. *Respir Physiol* 123: 201–213, 2000.

Strohl KP, Thomas AJ, St Jean P, Schlenker EH, Koletsky RJ, Schork NJ. Ventilation and metabolism among rat strains. *J Appl Physiol* 82: 317–323, 1997.

Thoby-Brisson M, Karlen M, Wu N, Charnay P, Champagnat J, Fortin G. Genetic identification of an embryonic parafacial oscillator coupling to the preBötzinger complex. *Nat Neurosci* 12: 1028–1100, 2009.

Tian GF, Peever JH, Duffin J. Bötzinger-complex, bulbospinal expiratory neurones monosynaptically inhibit ventral-group respiratory neurones in the decerebrate rat. *Exp Brain Res* 124: 173–180, 1999.

Tort AB, Kramer MA, Thorn C, Gibson DJ, Kubota Y, Graybiel AM, Kopell NJ. Dynamic cross-frequency couplings of local field potential oscillations in rat striatum and hippocampus during performance of a t-maze task. *Proc Natl Acad Sci USA* 105: 20517–20522, 2008.

Winter SM, Fresemann J, Schnell C, Oku Y, Hirrlinger J, Hülsmann S. Glycinergic interneurons are functionally integrated into the inspiratory network of mouse medullary slices. *Pfluegers* 458: 459–469, 2009.

Wittmeier S, Song G, Duffin J, Poon CS. Pacemakers handshake synchronization mechanism of mammalian respiratory rhythmogenesis. *Proc Natl Acad Sci USA* 105: 18000–18005, 2008.

Zhou D, Huang Q, Fung ML, Li A, Darnall RA, Nattie EE, St John WM. Phrenic response to hypercapnia in the unanesthetized, decerbrate, newborn rat. *Respir Physiol* 104: 11–22, 1996.